



WINNIPEG '96

GEOLOGICAL ASSOCIATION OF CANADA - MINERALOGICAL ASSOCIATION OF CANADA
ASSOCIATION GÉOLOGIQUE DU CANADA - ASSOCIATION MINÉRALOGIQUE DU CANADA
JOINT ANNUAL MEETING - RÉUNION ANNUELLE CONJOINTE
27-29 MAY/MAI 1996 - THE UNIVERSITY OF MANITOBA

FIELD TRIP GUIDEBOOK

GEOLOGY OF THE LAC DU BONNET BATHOLITH, INSIDE AND OUT: AECL'S UNDERGROUND RESEARCH LABORATORY, SOUTHEASTERN MANITOBA (FIELD B5)

by

R. Everitt, J. McMurray, A. Brown and C. Davison

1. AECL, Whiteshell Laboratories, Pinawa, Manitoba, R0E 1L0

Recommended citation: R. Everitt, J. McMurray, A. Brown and C. Davison
Geology of the Lac du Bonnet Batholith, Inside and Out: AECL's Underground
Research Laboratory, Southeastern Manitoba - Field Trip Guidebook B5,
Geological Association of Canada/Mineralogical Association of Canada Annual
Meeting, Winnipeg, Manitoba, May 27-29, 1996.

© Copyright Geological Association of Canada, Winnipeg Section



Electronic Capture, 2008

The PDF file from which this document was printed was generated by scanning an original copy of the publication. Because the capture method used was 'Searchable Image (Exact)', it was not possible to proofread the resulting file to remove errors resulting from the capture process. Users should therefore verify critical information in an original copy of the publication.

© 1996:

This book, or portions of it, may not be reproduced in any form without written permission of the Geological Association of Canada, Winnipeg Section. Additional copies can be purchased from the Geological Association of Canada, Winnipeg Section. Details are given on the back cover.

CONTENTS

INTRODUCTION	1
LAC DU BONNET BATHOLITH	1
Regional Setting	1
Lithology	4
Structural Geology	6
Geochronology and Tectonics	7
Geochemistry	9
UNDERGROUND RESEARCH LABORATORY (URL)	10
Litho-structural Domains	11
Auto-intrusives	15
Fracture Zones	16
Fracture Domains	17
Relation Between Fractures and Stress Fields	19
Hydrogeology	21
Groundwater Geochemistry	23
DESCRIPTION OF FIELD TRIP STOPS	25
Stop 1. Overview from hillside NW of URL parking lot	25
Stop 2. Fractured xenolithic granite in thrust fault (FZ3) hangingwall	26
Stop 3. Moderately fractured granite, epidote-filled fractures, and surface exposure of tip of granodiorite dyke swarm	27
Stop 4. Sparsely fractured granite, pegmatite dykes, strain measurements	27
Stop 5. URL headframe	28
Stop 6. (Optional) Fracture Zone 3 in the shaft, 120 m depth	28
Stop 7. Xenolithic granite and subvertical fractures at the 130 Level	31
Stop 8. (Optional) Litho-structural domains in the shaft, 150 m depth	31
Stop 9. Fracture Zone 2.5 in the shaft, 215 m depth	33
Stop 10. 240 Level Station: Geology of the 240 Level	34
Stop 11. (Optional) Transition from fractured to unfractured granite near FZ2.5	38
Stop 12. Correlation between fractures, in situ stresses, and hydraulic transmissivity at the 240 Level	40
Stop 13. Special excavation techniques, prominent subvertical fracture in Room 209 (Quarried Block Fracture Migration Experiment)	43
Stop 14. (Optional) Fracture Zone 2 in the shaft, 270 m depth	44
Stop 15. Granodiorite dykes in grey granite, excavation damage fractures at the 300 Level	48
Stop 16. 420 Level Station: Geology of the 420 Level	49
Stop 17. Excavation damage study, Room 405`	53
Stop 18. Mine-by Experiment, Room 415	55
ACKNOWLEDGMENTS	58
REFERENCES	58

LIST OF FIGURES

- Figure 1. Subdivisions of the Superior Province (after Card and Ciesielski 1986).
- Figure 2. Location of the Lac du Bonnet Batholith and nearby similar intrusions of the Winnipeg River Subprovince in southeastern Manitoba.
- Figure 3. Distribution of intrusive phases in the Lac du Bonnet Batholith (after Cerny et al. 1987), and generalized surface geology of the URL lease site (after Brown and Soonawala 1982).
- Figure 4. Surface facilities, ventilation raise, shaft, shaft stations, and major testing levels in the Underground Research Laboratory.
- Figure 5. Modal classification (IUGS 1973) of intrusive phases of the Lac du Bonnet Batholith. Samples are from the URL lease site.
- Figure 6. Generalized block models through the URL lease showing low-dipping fracture zones and location of litho-structural and fracture domains (from Everitt et al. 1990).
- Figure 7: Unrolled perimeter map from URL access shaft (288 m depth) showing the influence of a narrow xenolithic horizon on the location and orientation of Fracture Zone 1.9.
- Figure 8. Variation in fracture frequency with granite fabric type, based on data from a 240-m scan-line down the URL upper vent raise.
- Figure 9. Generalized extent and geometry of granodioritic dyke swarm at the URL.
- Figure 10. Summary of fracture domains as seen in the URL access shaft.
- Figure 11. Comparison of vertical versus horizontal trace lengths of subvertical fractures.
- Figure 12. In situ stress domains in the URL in relation to the fracture domains (stress data from Martin 1989).
- Figure 13. Characteristic hydraulic pressure conditions as measured prior to excavation (after Davison 1982).
- Figure 14. Variation in WRA groundwater chemistry with depth for: (A) total dissolved solids (TDS) and (B) chlorinity.

- Figure 15. Schematic representation of groundwater compositions at the URL lease site, showing groundwater flow paths and geochemical patterns in fracture zones.
- Figure 16. Panoramic view (Stop 1) showing the relationship between surface topography, the fault zone outcrop, and geology at the URL.
- Figure 17. Outcrop of sheared fine-grained granite zones, with left lateral strike-slip movement and pegmatitic terminations (Stop 4). The outcrop was also the location for recoverable strain measurements.
- Figure 18. Simplified geological map of the shaft walls at Fracture Zone 3 (Stop 6).
- Figure 19. Simplified geological map of 3 litho-structural domains in the URL shaft between 135 and 170 m depth (Stop 8).
- Figure 20. Simplified geological map of the shaft walls at Fracture Zone 2.5 (Stop 9).
- Figure 21. Simplified geological cross section through the 240 Level, here indicated by Room 209, showing its location relative to Fracture Zones 2 and 2.5 (Stop 10).
- Figure 22. Simplified geological map of the 240 Level showing the type and locations of fractures.
- Figure 23. Location of fracture zones and alteration haloes in relation to the access tunnels for the MFR Experiment (Stop 11).
- Figure 24. Variations in permeability within Fracture Zone 2.
- Figure 25. Variations in hydraulic conductivity within Fracture Zone 2 in the area below the 240 Level. Contours show the elevation (m) for the top of Fracture Zone 2.
- Figure 26. Map of the litho-structural domains hosting Fracture Zone 2 (Stop 12).
- Figure 27. Areas of core discing and measured normal stresses (Stop 12).
- Figure 28. Geology and excavation damage in a tunnel segment cut by diamond wire saw at the 240 Level (Stop 13): (A) southwest wall adjacent to full-face blast round, (B) northeast wall adjacent to pilot-and-slash-round.
- Figure 29. Simplified geological map of Fracture Zone 2 as seen in the URL access shaft (Stop 14).

Figure 30. General structure and total offset of Fracture Zone 2 as seen in a cross section normal to its strike (Stop 14).

Figure 31. Simplified geological map showing the excavation damage at the 300 Level (Stop 15).

Figure 32. Simplified geological map of the 420 Level Crib Raise showing litho-structural domains (Stop 16).

Figure 33. Perimeter map showing excavation damage breakout contours and general fracture orientation in the Room 405 borehole (Stop 17).

Figure 34. Geological map of the Mine-by Experiment test tunnel (Stop 18).

INTRODUCTION

The Lac du Bonnet Batholith is one of many late-tectonic granites emplaced in the western Superior Province of the Canadian Shield towards the end of the 2760-2670 Ma Kenoran event (McCrank et al. 1981; Davis et al. 1986; Stone et al. 1989). It is a relatively undifferentiated and partly foliated porphyritic granite-granodiorite consisting, like many other Archean batholiths, of broadly related but not sequentially fractionated intrusions (Cerny et al. 1987).

In the late 1970's, the Lac du Bonnet Batholith was one of five research areas that were selected for investigations by Atomic Energy Canada Limited (AECL) as part of a broad program to assess the concept of nuclear waste disposal in plutonic rocks of the Canadian Shield (Whittler 1987). The objectives of the field investigations were to develop the methodology and instrumentation for screening and characterizing sites and to develop an understanding of the field parameters that control fluid flow, mass transport, and geomechanical response in plutonic rock. In the Environmental Impact Statement submitted to the federal government on the concept for disposal of Canada's nuclear fuel waste (AECL 1994), the geotechnical database on the Lac du Bonnet Batholith was used in the case study for an illustrative assessment of the long-term safety of a hypothetical disposal facility (Davison et al. 1994; Goodwin et al. 1994).

The Lac du Bonnet Batholith has been the most extensively studied of the AECL field research areas. Surface and airborne field studies were complemented by a large drilling program of more than 130 boreholes, most of them cored, to depths of up to 1100 m to develop a better understanding of the geology of the batholith and to develop and test a conceptual model of the groundwater flow system. Detailed information about subsurface characteristics of the Lac du Bonnet Batholith also is obtained from the Underground Research Laboratory (URL), which was constructed by AECL to a depth of 443 m below the surface to provide a realistic environment in which to conduct in situ geotechnical experiments in granitic rock. In addition to developing a clearer understanding of the geology, specific studies at the URL include those on groundwater movement and chemistry, in situ stress conditions, temperature-dependent and time-dependent deformation characteristics and failure behaviour of the granite, colloid migration, the absorption properties of the minerals in the host rock and fractures, development of mining techniques that minimize excavation damage, and tests of the performance of sealing and backfilling materials (Martin and Simmons 1992). No nuclear fuel waste is used for research at the site.

LAC DU BONNET BATHOLITH

Regional Setting

The Lac du Bonnet Batholith is located on the western margin of the Superior Province (Figure 1), which comprises a number of east-west trending litho-tectonic subprovinces in northwestern Ontario and eastern Manitoba (Card and Ciesielski 1986). The batholith is associated temporally and spatially with several other felsic bodies of roughly the same exposed size and age in the Winnipeg River Subprovince,

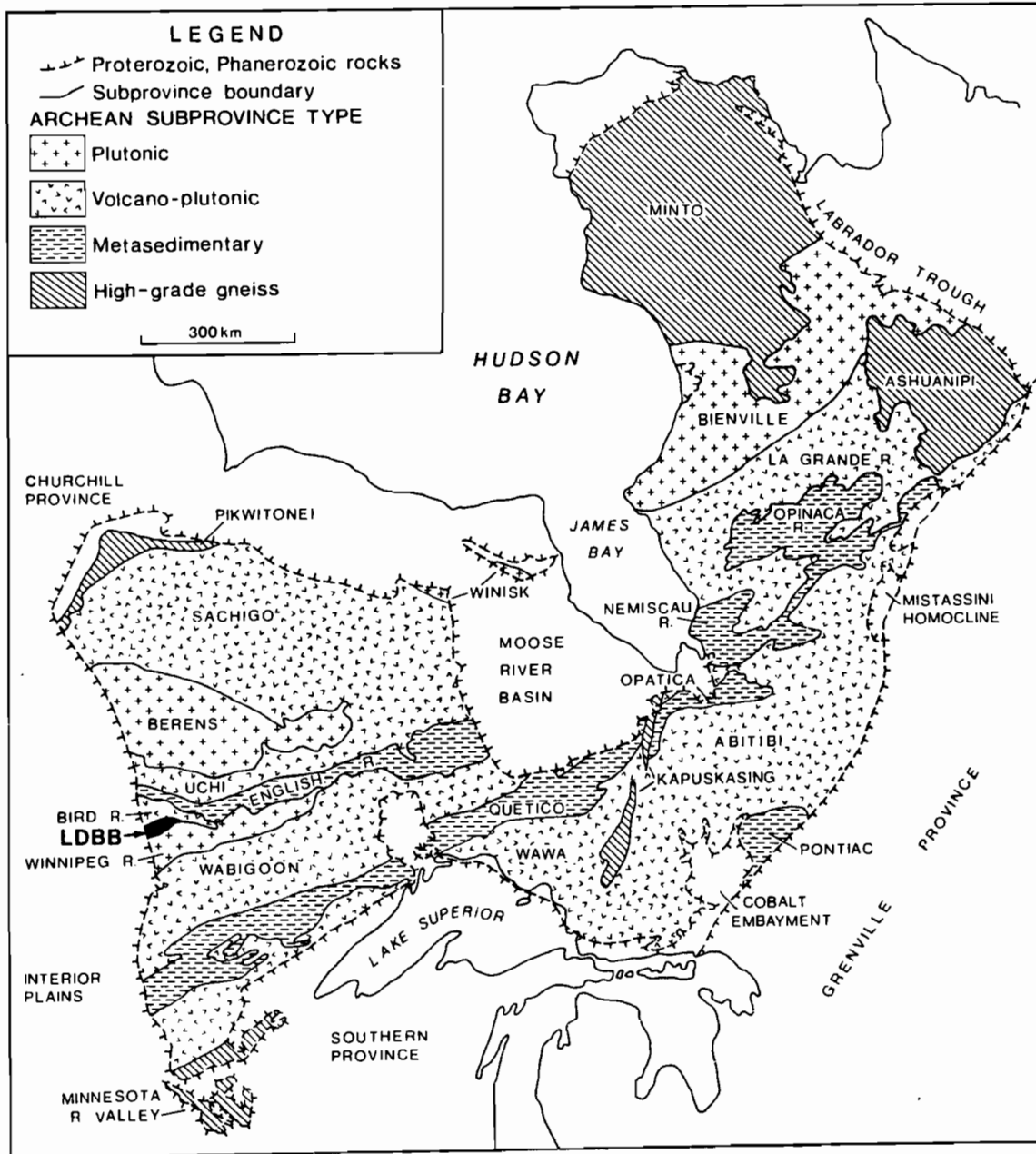


Figure 1. Subdivisions of the Superior Province (after Card and Ciesielski 1986). LDBB, Lac du Bonnet Batholith

including the Betula Lake and Medika plutons (Figure 2). The relatively sparsely fractured characteristics of large portions of these bodies, and of the Lac du Bonnet Batholith, are attributed at least in part to their intrusion at or near the end of regional deformation (Brown et al. 1989), to prolonged cooling--which delayed the onset of brittle deformation--due to the size of the bodies and their proximity to each other, and to the distance separating the intrusions regionally from later tectonic events in the Superior Province (Everitt et al. 1990).

To the north, the batholith is in sharp contact with a narrow belt of metavolcanic rocks in the Bird River Greenstone Belt, and to the south it is in gradational contact with gneisses and migmatites of the Winnipeg River Subprovince (Beakhouse 1977). From a tapered eastern margin, surface exposures of the batholith extend westward 85 km. West of the Winnipeg River, the batholith is largely concealed by glacio-lacustrine sediments and by Paleozoic carbonate rocks; however, geophysical data indicate that the granitic rocks extend westward at least another 20 km (McRitchie 1971).

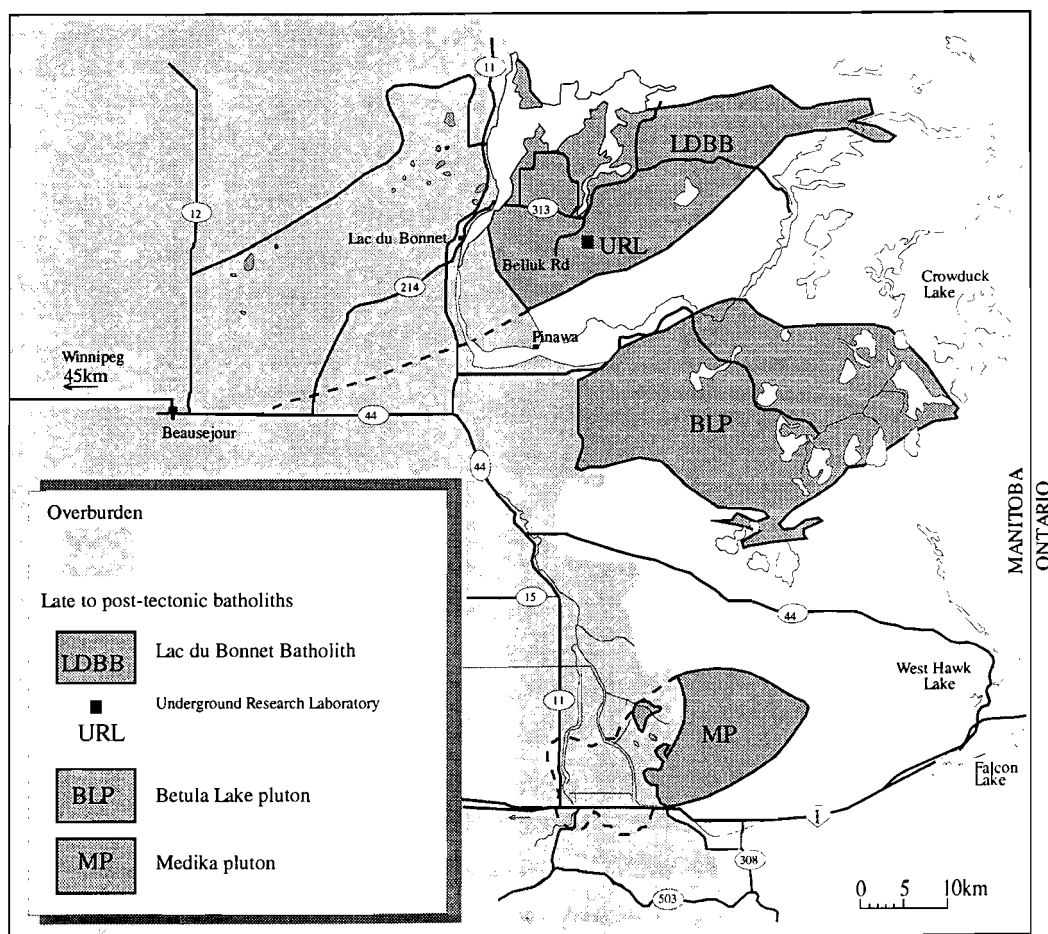


Figure 2. Location of the Lac du Bonnet Batholith and nearby similar intrusions of the Winnipeg River Subprovince in southeastern Manitoba.

Lithology

On the basis of mineralogy, texture, intrusive relationships, and geochemistry, Cerny et al. (1987) identified five phases of the Lac du Bonnet Batholith (Figure 3), in order of decreasing relative age:

- 1) gneissic hornblende-biotite tonalite (possibly xenoliths)
- 2) gneissic porphyritic hornblende-biotite granodiorite
- 3) gneissic to undeformed leucogranite
- 4) biotite granite (the main phase of the batholith)
- 5) late-tectonic biotite granodiorite dykes

In terms of field relations, the oldest phase identified is strongly foliated hornblende-biotite tonalite. Modally and chemically distinct from all the other rock types, it occurs only as widespread but relatively minor enclaves in other rock types. McCrank (1985) and Stone et al. (1984) mapped exposures of this phase in the late-tectonic biotite granite as xenolithic material, and Cerny et al. (1987) noted that its inclusion in the batholith sequence is arbitrary.

The two other early phases are restricted in occurrence to the eastern wedge of the batholith (Figure 3), where they exhibit a structural complexity not evident in the main portion of the batholith. The gneissic hornblende-biotite granodiorite contains megacrysts of plagioclase and K-feldspar up to 15 mm in length. It is intruded by the leucogranite, which is moderately to strongly foliated. The leucogranite is associated geochemically and spatially with abundant interior pegmatites and with an evolved set of pegmatites in the adjacent country rocks (Cerny et al. 1981).

Most surface exposures of the batholith consist of late-tectonic biotite-bearing granite. Porphyritic biotite granite, described as porphyroblastic by Cerny et al. (1987), is dominant in the central portion of the batholith and accounts for about one-fourth of the exposures. Equigranular granite is more common near the margins.

The biotite granite has been subdivided into additional lithological units on the basis of other textural and modal variations (Figure 3, inset) such as colour and biotite content (e.g., Stone et al. 1984; McCrank 1985; Brown et al. 1989), and it commonly shows two or three faintly different variations on the scale of a single outcrop. These variations are classified and described in more detail below, in the context of the geology of the URL lease site and its vicinity.

The present topographic surface of the batholith is thought to be close to the original roof zone of the intrusion. Pink, hematite-bearing granite predominates to depths of about 200 m, below which the dominant phase is grey magnetite-bearing granite, similar to the pink granite except for a lower $\text{Fe}_2\text{O}_3/\text{FeO}$ ratio. The "pinking" appears to be partly primary in origin, partly deuteric, and partly due to paleoweathering (late groundwater-induced alteration). Gascoyne and Cramer (1987) suggested that the colour difference was primary, resulting from increased $f(\text{O}_2)$ and $f(\text{H}_2\text{O})$ in the upper part of the crystallizing body. At the least, this process may be represented in rare examples where grey granite is crosscut by pink pegmatitic or porphyroblastic masses. However, where pink granite is found below 200 m, the colour change consistently is associated with alteration in and around fractures. Within the interiors of unfractured pegmatitic masses, the presence of hematite along grain boundaries,

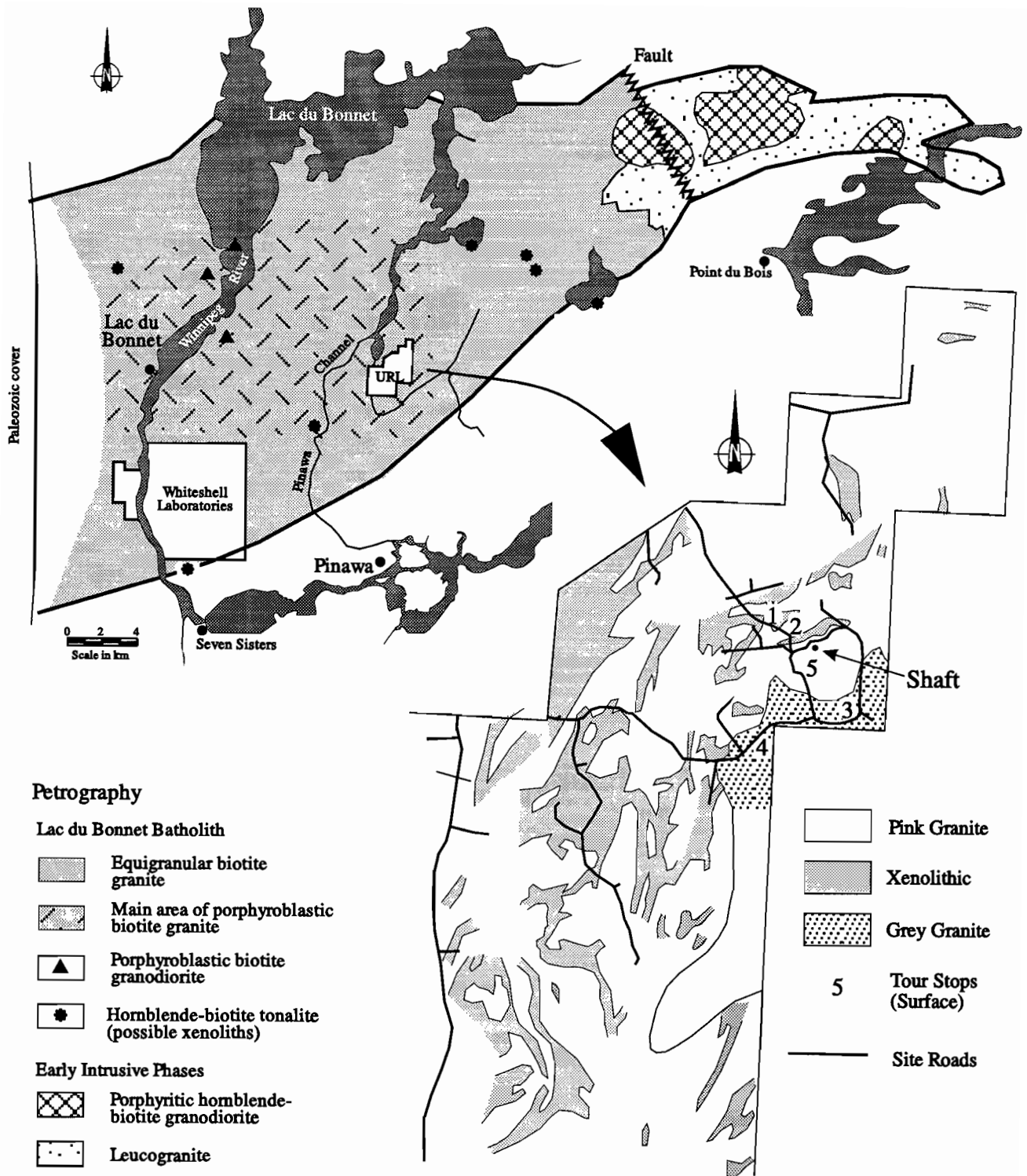


Figure 3. Distribution of intrusive phases in the Lac du Bonnet Batholith (after Cerny et al. 1987), and generalized surface geology of the URL lease site (after Brown and Soonawala 1982). Numbers 1-5 on inset map refer to location of above-ground field trip stops.

microcracks, and mineral cleavages is attributed to deuteric alteration (Everitt and Brown 1987). The spatial distribution of "pinking" and variations in its intensity suggest that the colour change resulted from one or more episodes of hydrothermal alteration along the pervasive network of open fractures in the upper 200 m of the batholith (Brown et al. 1989).

Late-tectonic, fracture-filling dykes of biotite granodiorite that intrude the biotite granite in the central part of the batholith are the youngest of the major phases recognized by Cerny et al. (1987). Although surface exposures are sparse, the extent and proportion of granodiorite dykes increase progressively with depth at the URL. The granite is also intruded by minor aplites and by numerous minor pegmatite dykes, particularly near the batholith margins. Irregular pegmatitic masses, and porphyroblastic schlieren (Cerny et al. 1987), occur throughout the biotite granite but are commonly associated with xenolith-rich zones (McCrank 1985; Everitt and Brown 1986). Various auto-intrusive felsic dykes are widespread but minor.

Structural Geology

Geological and geophysical evidence indicate that the northern contact of the batholith dips to the south at a relatively low angle (Brown et al. 1995). Drilling and geophysical surveys across the batholith contact suggest that the southern contact of the pluton dips outwards at an angle of 50-70°. The total volume of the batholith, based on estimated thickness (Brisbin 1979; MacLeod 1980; Tomsons et al. 1995) and dip of contacts, is between 9,060 km³ and 45, 000 km³ (Stone et al. 1989). In the vicinity of the URL, the distribution of xenolithic and schlieric layers in the granite suggests that the batholith was intruded locally along planes in gneissic host rock, then gently folded by diapiric rise (Brown et al. 1989).

Partly as a consequence of its large volume and its regional setting, the Lac du Bonnet Batholith cooled slowly and responded to deformation in a ductile manner during much of its history of crystallization and cooling (Kamineni et al. 1990a; Stone et al. 1989). With the exception of some strike-slip faults, brittle deformation appears to have been limited mainly to metre-scale displacements on chloritic thrust faults, most of which are concealed by overburden in linear valleys and have low to intermediate ESE, ENE, or WNW dips (Kamineni et al. 1990b). Discontinuities were subsequently rejuvenated without significant modification to the fracture style and extent. In general, except near the surface the batholith has been relatively stable since emplacement of the main phase, which is reflected in the low fracture intensity and the simplicity of fracture-filling minerals throughout the batholith (Stone et al. 1989).

Large-scale faulting is rare, limited primarily to a NW-striking fault in the eastern part of the intrusion (Trueman 1980) that offsets the northern contact of the batholith and forms a contact between the early leucogranite and the main phase biotite granite (Figure 3). Several large-scale lineaments, oriented ENE, are visible on satellite imagery. The ENE orientation of these lineaments coincides with the long axis of the batholith and with the structural fabric of the regional metamorphic rocks, and it is the main orientation of many small-scale fractures throughout the batholith.

Subvertical fractures are common in outcrop. These are long and straight and divide the rock into rectangular blocks that are eroded to form a stepped topography

marked by subvertical escarpments and flat to gently sloping outcrops (Stone et al. 1984). Subvertical fractures are rare below a depth of about 200 m, below which they are limited to the margins of low-dipping thrust faults and splays, or to unusual rock types such as dykes. Fracture zones conform to gross mineralogical or structural layering within the rock (Everitt and Brown 1986).

In large low-dipping fracture zones observed in the URL, hydrothermal alteration has resulted in a second zone of "pinking" superimposed on the primary zone adjacent to the fractures. More recent alteration in these fractures has bleached the rock and, where intensive, has formed low-temperature mineral assemblages. U-series disequilibria for some of these mineral assemblages indicate isotopic disturbance within the last 10^5 a (Gascoyne and Cramer 1987).

Subvertical fractures are grouped into those striking NNE (015° - 020°), those striking ESE (110° - 130°), and those striking SSE (160° - 170°). Locally significant groups strike S (180°) and NE (035°). The first two groups show many characteristics of extension fractures, such as irregularity and lens-shaped infilling. Unequivocal right-hand strike-slip movement is visible on fractures striking SSE; left-hand strike slip movement occurs on fractures striking NE. These observations suggest a NNE-trending compressive stress axis at the time of fracturing, similar to the stress field during the formation of later pegmatite dykes and quartz veins. (Brown et al. 1989). In general, subvertical fractures are partially or completely filled with a combination of chlorite, iron oxides, carbonates, and clay minerals.

Low-intermediate-dipping fractures (10° - 30°) are also common at surface and are associated with fault zones in the subsurface. These fractures and the subsurface fault zones are concordant at the URL with the mesoscopic-scale compositional layering of the batholith (Everitt et al. 1987). Exposures in the shaft of the URL, for example, show that the strongly banded margins of xenolith-rich granite and associated pegmatoidal lenses exerted a strong control on the localization of low-dip thrust faulting and subvertical fractures.

Geochronology and Tectonics

Zircon U-Pb ages in the Winnipeg River Subprovince span a relatively long and complex Archean history of about 500 Ma (Beakhouse 1985; Beakhouse et al. 1988; Corfu 1988). Late- to post-kinematic granitoids derived by crustal melting of older rocks are widespread in the Superior Province (Thurston 1991) and were emplaced between 2705 and 2660 Ma (Beakhouse et al. 1988). The Lac du Bonnet Batholith, with a U-Pb zircon age of 2665 ± 20 Ma (Krogh et al. 1976), was emplaced near the end of this interval.

The Rb-Sr systematics of the Lac du Bonnet Batholith have been investigated by a number of studies (Table 1). A Rb-Sr isochron for the leucogranitic rocks in the eastern part of the batholith gives $t = 2550 \pm 190$ Ma (Cerny et al. 1987); the high relative error (more than 7 percent of the indicated age) is attributed to the high Rb/Sr ratio of the leucogranite and to the high degree of recrystallization in the foliated rock. Whole-rock analyses of biotite granite have yielded isochrons of 2621 ± 162 Ma (Penner and Clark 1971; Farquharson 1975) and 2603 ± 97 Ma (Cerny et al. 1987). Kamineni et al. (1990b) analyzed 16 samples of unaltered biotite granite from drill cores at the URL

over a range of depths from 44 to 1068 m below the surface and obtained a whole-rock Rb-Sr age of 2568 ± 23 Ma.

Kamineni et al. (1990b) also obtained four internal Rb-Sr isochrons based on mineral separates of unaltered granite (plagioclase, microcline, biotite) from cores at depths between 57 m and 1068 m. In all four cases the high Rb of biotite controlled the slope of the isochrons and gave Early Proterozoic ages of around 2300 Ma (Table 1). The biotite dates are progressively younger with depth, indicating that Rb-Sr systematics were influenced by cooling of the batholith. In contrast, microcline/whole-rock isochrons of 2206 ± 86 and 2298 ± 48 Ma from strongly altered and oxidized granite in a fracture zone record low-temperature hydrothermal alteration along one of the subsurface thrust faults in the batholith, and a steeply dipping epidote-bearing fault zone near the eastern margin gives an age of 2350 ± 60 Ma. The overlap in ages from the biotite (in pristine rock) and fault zone (altered rock) data indicate that fault-related deformation occurred prior to the regional thermal stabilization of the batholith. This points to a long cooling history for the intrusion (Kamineni et al. 1990a). Furthermore, the timing of the faulting and other brittle structures in the Lac du Bonnet Batholith show that the internal disturbance of the Superior Province did not terminate with plutonism at the end of the Kenoran orogeny, but continued intermittently for at least several hundred million years, possibly in response to events taking place beyond the margins of the craton (Osmani 1992).

Table 1: Geochronological data for the Lac du Bonnet Batholith

Material/method	Age (Ma) ¹	Depth of sample (m)	Reference
Zircon (U-Pb)	2665 ± 20	surface	Krogh et al. 1976
Biotite granite (Rb-Sr)	2621 ± 162	surface	Penner and Clark 1971; Farquharson 1975
	2603 ± 97	surface	Cerny et al. 1987
	2568 ± 23	44 - 1068	Kamineni et al. 1990b
Leucogranite (Rb-Sr)	2550 ± 190	surface	Cerny et al. 1987
Fault zone epidotized and cataclastic rocks (Rb-Sr)	2206 ± 86	FZ2 ²	Kamineni et al. 1990b
	2298 ± 48	FZ2	
Mineral separates from "pristine" biotite granite (Rb-Sr)	2308 ± 48	57	Kamineni et al. 1990b
	2340 ± 36	326	
	2343 ± 49	922	
	2270 ± 47	1068	
Near-surface altered rock adjacent to fractures ($^{234}\text{U}/^{238}\text{U}$; $^{230}\text{Th}/^{234}\text{U}$)	appx. 0.1	near-surface	Gascoyne and Cramer 1987

¹ all errors quoted at 2 sigma

² Fracture Zone 2

Gascoyne and Cramer (1987) found disequilibrium values of $^{234}\text{U}/^{238}\text{U}$ and $^{230}\text{Th}/^{234}\text{U}$ in altered rock adjacent to fractures, in a surface sample and in drill core samples at a depth of about 150 m, indicating that near-surface uranium has been mobilized in recent geological time (within the last 10^5 a) but that Th has remained relatively immobile. Apparently unaltered rock, slightly farther from the fractures, has lost appreciable U but is no longer in disequilibrium, indicating that the loss occurred at least a million years ago and perhaps much earlier, during deuteric or hydrothermal alteration. In the same study, a drill core sample from the batholith from a depth of 730 m showed little evidence of U mobilization, either recently or ancient. When the U-series results are correlated with observed concentrations and isotopic activity ratios of U in groundwaters sampled from the same or adjacent fractures, samples from highly altered rubble in the fractures show both excesses and deficiencies of ^{234}U and ^{230}Th in neighboring locations, possibly due to the presence of a redox front whose position is controlled by modern groundwater composition.

Geochemistry

Detailed geochemical data for the Lac du Bonnet Batholith are presented by Cerny et al. (1987). The various intrusive phases of the batholith span a relatively narrow range of silica content, with SiO_2 from about 64 wt.% for early, foliated hornblende-biotite granodiorite to about 75.5 wt.% for early leucogranite; the main phase biotite granite has average SiO_2 of about 73 wt.% and Al_2O_3 of about 14 wt.%. Except for the early and possibly xenolithic tonalite, the intrusive phases of the batholith are of overlapping modal compositions, and all are calc-alkaline to slightly alkaline on a Peacock diagram. Oxygen isotope data for the batholith show no significant variation by rock type. The mean $\delta^{18}\text{O}$ values for the various phases are very similar, ranging from +7.8 to +8.4 per mil. Nevertheless, each phase defines specific compositional areas on variation diagrams, with no direct chemical link between the rock types. All phases are strongly enriched in LREE, but they have variable HREE contents consistent with each phase.

On the basis of its oxygen and Sr isotopic characteristics, Cerny et al. (1987) concluded that the granitic main phase of the batholith could not have formed by substantial melting of sedimentary supracrustal rocks, although small degrees of melting of a less potassic source such as LILE-depleted tonalitic crust could generate the weakly Eu-depleted and strongly HREE-depleted REE assemblages by leaving at depth a plagioclase and hornblende-rich residue. However, the original biotite granite magma also would have been modified by the separation of a volatile-saturated pegmatite melt, and by the altered metasediments in the source region, the presence of which would be required to account for the observed values of oxygen isotopes and of K_2O .

UNDERGROUND RESEARCH LABORATORY (URL)

In 1980, AECL acquired a lease on a 3.8 km² area of the Lac du Bonnet Batholith for construction of the URL as part of the geoscience research for the Canadian Nuclear Fuel Waste Management Program. The site, chosen for the quantity of outcrops and its proximity to AECL's Whiteshell Laboratories, is 2.5 km north of the southern contact of the batholith and 14 km east of the town of Lac du Bonnet (Figure 3).

The Lac du Bonnet Batholith is exposed in the subsurface in the URL by a vertical access shaft that extends to a depth of 443 metres and by two major testing levels at depths of 240 and 420 metres, each of which is a series of tunnels that extend more-or-less horizontally for several hundred metres in a loop from the access shaft (Figure 4). Access by hoist to the 240 Level is provided by a rectangular 2.8 m x 4.9 m shaft with timber sets and to the 420 Level by a 4.6-m diameter circular shaft with steel sets. Raise-bored ventilation shafts, a timber-framed raise at the 420 Level, and small shaft stations in the main access shaft at depths of 130 m and 300 m also provide exposures of the batholith at depth.

The excavations at the URL provide a cross section of the roof zone of the Lac du Bonnet Batholith, of two low-dipping thrust faults and associated splays, and of the subvertical intrablock fractures that flank the major faults. The roof zone is marked by deuteritic alteration and by shallow-dipping compositional layering. Low-dipping fractures, including thrust faults, parallel the large-scale compositional layering, and are generally confined to the contacts between massive leucocratic and foliated xenolithic litho-structural domains.

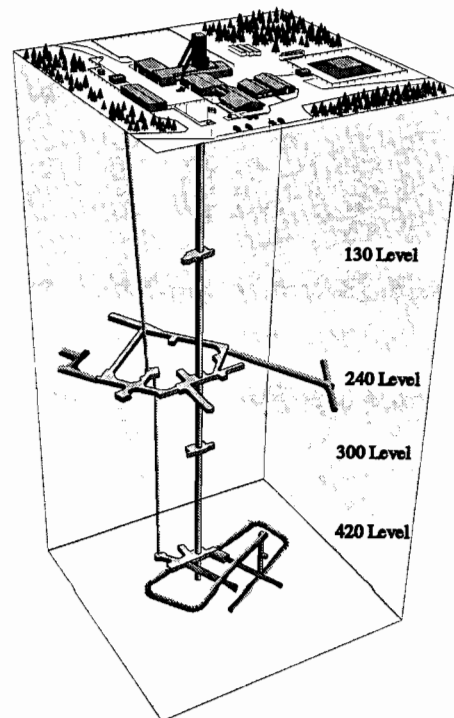


Figure 4. Surface facilities, ventilation raise, shaft, shaft stations, and major testing levels in the Underground Research Laboratory.

Litho-structural Domains

The dominant lithology at the URL is biotite-bearing granite, with lesser amounts of quartz monzonite and granodiorite (Figure 5), that is representative of the main rock type of the Lac du Bonnet Batholith. Outcrop-scale variations in colour, texture, and mineral content are more clearly defined in the subsurface. One of the most significant geologic results coming from the characterization of the URL was the discovery that the batholith is coarsely layered rather than homogeneous as suggested in outcrop elsewhere in the batholith. Xenolithic, leucocratic and heterogeneous zones within the eastern two-thirds of the URL lease define a large-scale NE-striking, SE-dipping layering (Figure 6). These layers, or litho-structural domains, are distinguished from each other on the basis of xenolith content, the relative abundance of late residual or metamorphic segregations, the presence of internal auto-intrusive contacts, and variations in mesoscopic fabric (massive, gneissic, schlieric, xenolithic, etc.) as well as by the orientation of their foliations.

The textural and compositional layering is clearly delineated in the URL shaft (Everitt and Brown 1986), where it has been shown to exert a strong control on the localization of low-dip thrust faulting (Figure 7). Fractures are the most common where

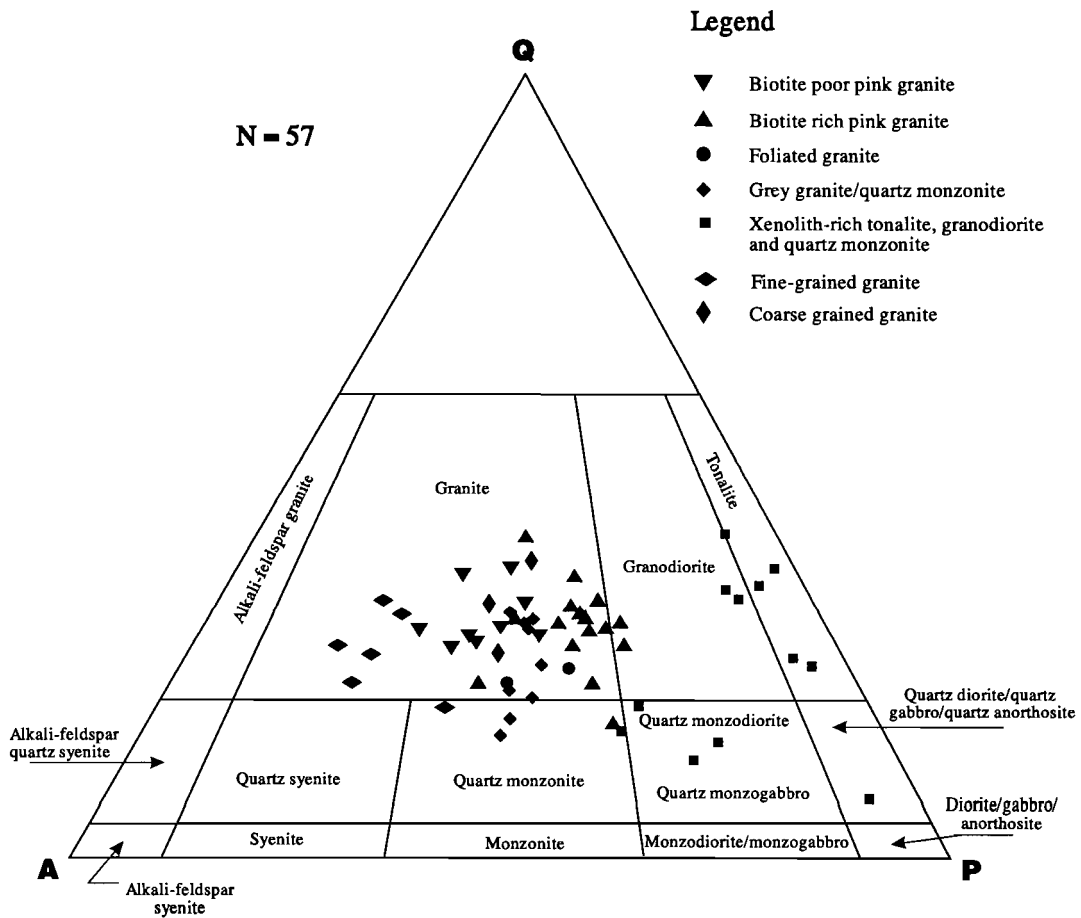


Figure 5. Modal classification (IUGS 1973) of intrusive phases of the Lac du Bonnet Batholith. Samples are from the URL lease site.

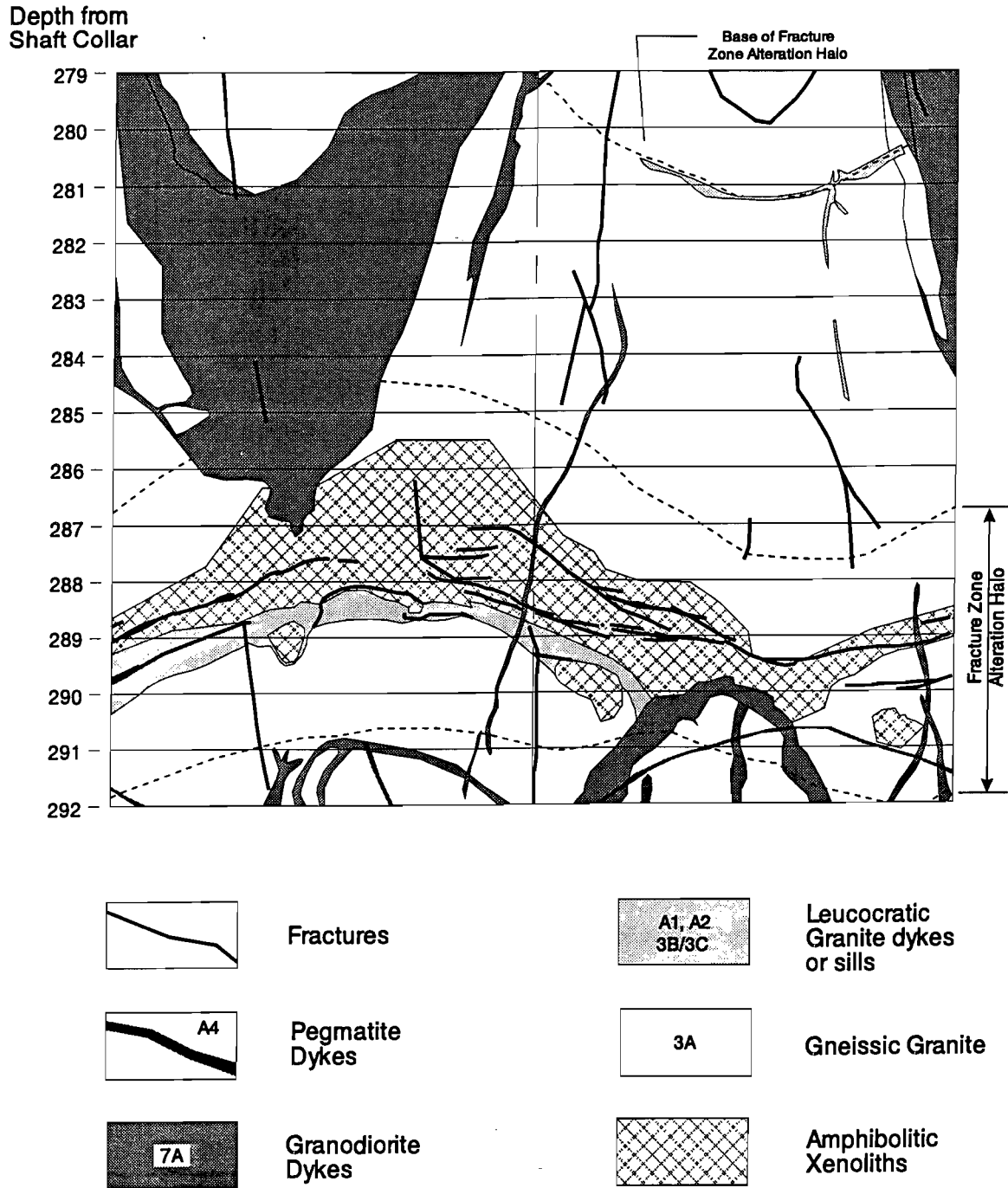


Figure 7. Unrolled perimeter map from URL access shaft (288 m depth) showing the influence of a narrow xenolithic horizon on the location and orientation of Fracture Zone 1.9.

layering is prominently developed in the granite (Figure 8). The subvertical fractures also vary with respect to the litho-structural domains in terms of fracture orientation, spacing, infilling, and other characteristics.

The litho-structural domains are not conspicuous at the surface, largely due to low topographic relief and the subhorizontal orientation of the layering. However, field mapping in the vicinity of the URL has identified a series of domes trending NNE in a long antiform (Brown and Soonawala 1982), outlined by bands of xenolith-bearing granite and associated pegmatoidal granite, that may represent surface expressions of litho-structural domains.

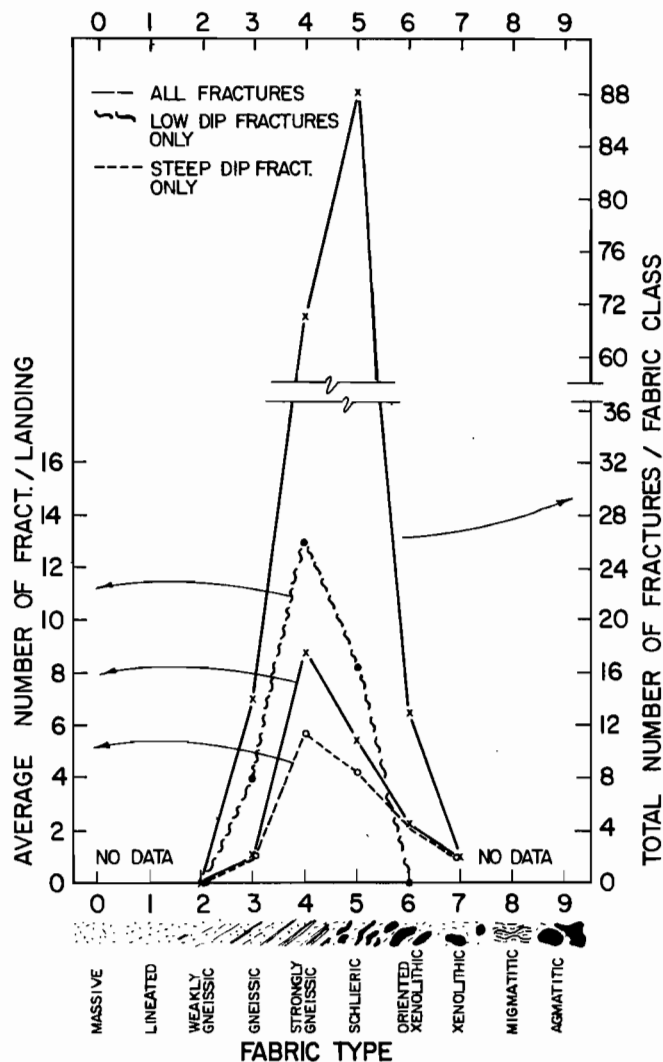


Figure 8. Variation in fracture frequency with granite fabric type, based on data from a 240-m scan-line down the URL upper vent raise.

Auto-intrusives

In the subsurface, four systems of dykes, sills, and recrystallized zones crosscut the main fabric types of the granite. In order of decreasing relative age, these intrusives consist of:

- rare early granitic dykes,
- early leucocratic segregations and metasomatized zones,
- granodioritic dykes, and
- minor late pegmatite-aplite dykes and their derivatives.

The last group is transitional with mineralized fractures in the batholith. This series of structures is thought to represent a continuous progression from late magmatic to post-magmatic hydrothermal events.

Of the dykes and sills that intruded the main granite, the granodioritic dyke swarm is the most extensive, and it has been traced in the subsurface through its intersection with boreholes and with the URL shaft (Figure 9). At surface, the swarm is represented mainly by narrow zones of minor alteration and deformation in the host granite. In the URL at the 130 Level Shaft Station and in the shaft at 200 m depth, the dyke swarm becomes better defined as biotitic schlieren or as fine-grained ductilely deformed zones that crosscut and offset compositional layering in the granite. The dykes increase in size and number with depth such that at the 240 Level, clearly defined dykes of strongly flow-banded, fine-grained granodiorite or granite are present,

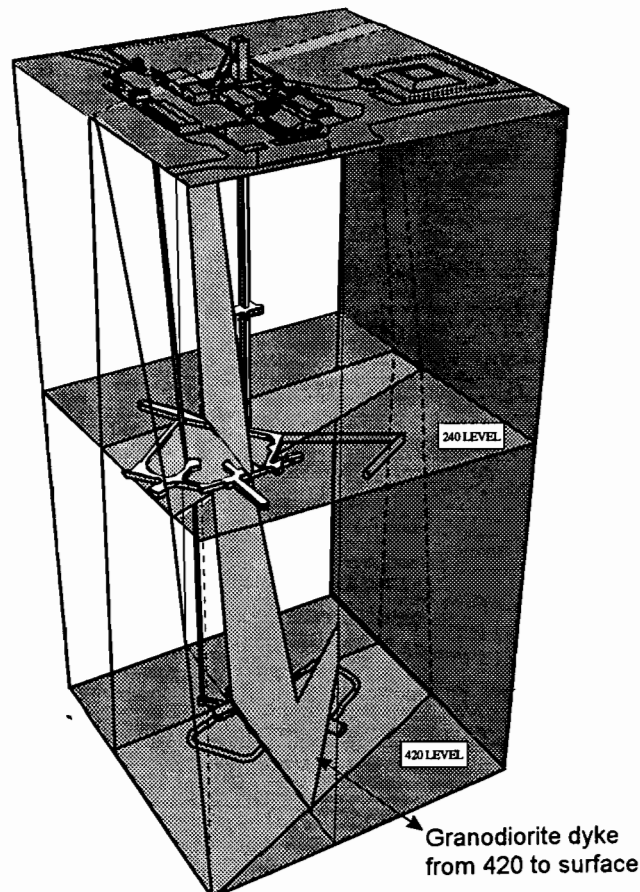


Figure 9. Generalized extent and geometry of granodioritic dyke swarm at the URL.

with an average dyke orientation of 160°/73° SW. In the deepest part of the URL, granodiorite dykes are the dominant rock type and attain widths of up to 15 m. Deformation in the tip region at and above the 240 Level was ductile, with the development of drag folds and local foliations, and local boudinage of the adjacent host rock and the dyke fillings, including quartz veins. Normal offset (west side down) was consistently developed to the depth of the 300 Level Shaft Station. At the 420 Level, seemingly inconsistent reverse dip-slip displacement may be due to rotation of blocks between individual dykes, as the proportion of dyke to host rock increases with depth.

Fracture Zones

The term “fracture zone” as originally employed at the URL (Davison 1982), referred to regional scale, low-dipping, variously permeable horizons that contained both low-dipping and steeply dipping fractures. Shaft mapping has shown that these fracture zones consist of thrust faults, each flanked by lesser fractures and by an alteration halo. The thrust faults have chloritic slip surfaces which grade into complex cataclasite zones where fault movement has been significant (on the order of metres). The cataclasites consist of recrystallized fault rubble cemented by a fine grained chlorite-carbonate matrix, and they are crosscut by chloritic slip surfaces, minor fractures, and seams of soft clay - goethite gouge. This assemblage is in varying stages of groundwater-induced decomposition.

During construction of the URL, a working definition was developed for distinguishing the fracture zones in boreholes, in order to avoid inadvertent intersection with the planned excavations. The boundaries of the fracture zones were arbitrarily defined as the last low-dipping fractures encountered in the hangingwall and footwall about either (1) the central cataclasite (rubble) zones(s), or (2) the centre of the zone as based on the relative number and character of fractures and alteration zones. Steeply dipping fractures were excluded from this definition, because shaft mapping has shown that these extend well beyond the actual low-dipping faults and associated fractures. The tops and bottoms so defined may be considered the limits within which the fracture zones vary in thickness, orientation and complexity.

Fracture Zone 1, the deepest fracture zone identified during site characterization, is not present in the area of the URL excavations. It terminates about 500 m up-dip from the excavations (Figure 7).

Fracture Zone 2, the deepest fracture zone intersected by the excavations, comprises a relatively simple system of conjugate shears and extension fractures (the cataclasite zone/chloritic fractures, and the antithetic hematite-filled fractures respectively). Displacement appears to have been reverse dip-slip only, with the overlying block moving 7.3 m to the northwest.

The fracture patterns for Fracture Zone 2.5 and Fracture Zone 3, which are located above Fracture Zone 2, are dominated by the same general arrangement of the major slip surfaces, but additional low-dipping and subvertical fracture sets are present. Overall, their geometry resembles two conjugate systems, superimposed to give orthorhombic symmetry, as described by Davis (1984). Reverse dip-slip (up to 1 m) dominates in these zones, but strike-slip and oblique slip lineations overprint the dip-slip lineation.

The fracture zones divide the rockmass into a number of tabular to wedge-shaped blocks. These blocks are crosscut by one or more sets of subvertical fractures, the pattern and frequency of which varies from one block (fracture domain) to the next. The factors influencing the pattern of intrablock fractures include the overall distance from the surface, the proximity to the bounding faults, and the local rock type. With increasing depth, the subvertical fractures become less frequent, less continuous, and simpler in pattern. They also become increasingly confined to the immediate margins of the fault zones or to lithological heterogeneities such as dykes.

Fracture Domains

Four domains of fractures have been identified from surface and subsurface mapping, and from drilling (Figure 7). Fracture Domain "A" extends from the surface to the base of Fracture Zone 3. Within this domain, the predominant NNE-striking subvertical set dips primarily to the NW (Figure 10). A NNW-striking set is less abundant, but individual fractures have been traced from surface to the top of Fracture Zone 3, a distance of almost 100 m. Other directions of fracturing, such as a NW to WNW subvertical set, are common near surface. Also present are non-systematic intrablock fractures, and other fractures related to either local fabrics or to surface influences. Low-dipping sheeting fractures have been encountered to a depth of 15 m from the surface but are not common. Chloritic low-dipping fractures exposed in the upper 15 m of the shaft show dip-slip lineations and are thought to be related to the major low-dipping thrust faults. Subvertical fractures are terminated against these chloritic fractures and against similar slip planes in Fracture Zone 3.

Fracture domain "B" extends from the base of Fracture Zone 3 to the base of Fracture Zone 2.5. The pattern of fracturing here is more ordered than for fracture domain "A" (Figure 10). Non-systematic or local fracture sets are minor in extent and number. The dominant near-vertical NNE-striking set is well defined, dipping NW or SE in approximately equal proportions. This set is largely confined to the upper and lower thirds of the fracture domain (i.e., its margins adjacent to the low-dipping fracture zones). The variety of infilling materials and the variability of this set about its mean orientation also increase as the bounding fracture zones are approached.

Fracture domain "C" extends from the base of Fracture Zone 2.5 to the top of Fracture Zone 2 (Figure 10). Fracture domain "D" encompasses the remainder of the area in the URL below Fracture Zone 2. Natural fracturing in this domain is largely confined to the immediate margins of the bounding fault zones, or to specific lithological heterogeneities such as dykes and leucocratic zones. It is largely unimodal, with a dominant subvertical NE-striking set, and a minor subvertical NW-striking set.

A comparison of the horizontal versus vertical trace lengths for the subvertical fractures is provided in Figure 11. The data are from surface outcrop (Stone et al. 1984) and the shaft mapping respectively. The ratio of horizontal to vertical trace length is roughly of 9:1. This appears to be due to a number of factors, including 1) the truncation of most subverticals against the low-dipping fractures of various types in the near-surface environment, 2) the truncation of the subverticals against the low-dipping thrust faults, 3) the tendency for the subverticals to be constrained by the low-dipping layering in the granite, and 4) fracture propagation under a horizontal σ_1 stress axis.

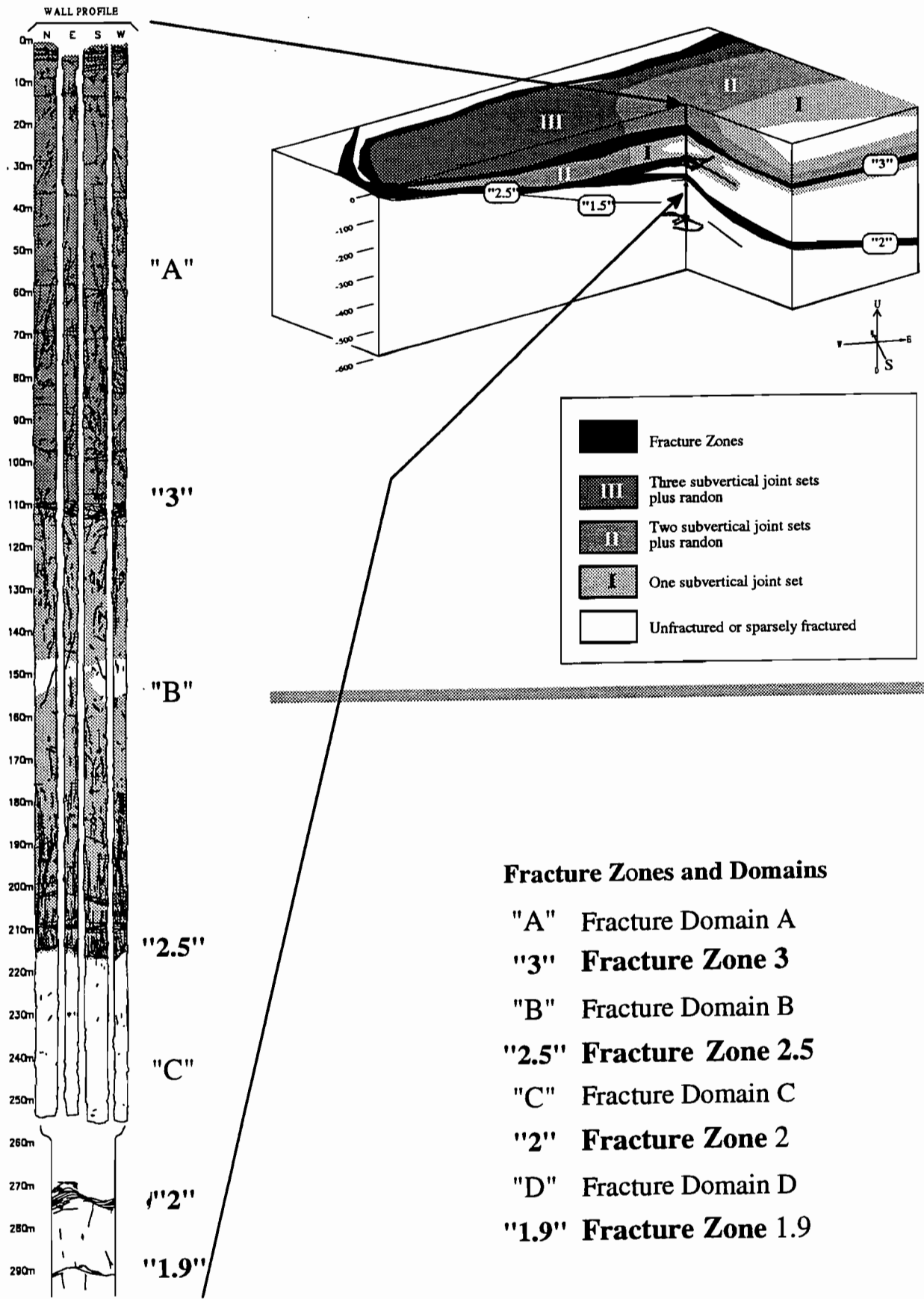


Figure 10. Summary of fracture domains as seen in the URL access shaft

FRACTURE LENGTH

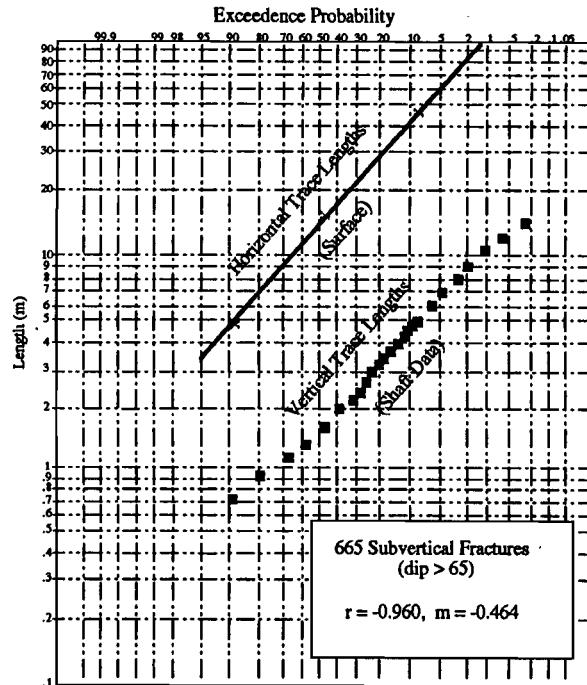


Figure 11. Comparison of vertical versus horizontal trace lengths of subvertical fractures. Statistics refer to the shaft data set.

Relation Between Fractures and Stress Fields

The differences in the structure of the fracture zones, and in the fracture domains between them, are explained using the model depicted in Figure 12. This model is based on the underground mapping, and on data from surface and underground boreholes in the URL vicinity, re-interpreted using the perspective provided by the shafts. This model may have wider application, but is one of several models under consideration for the regional scale.

The northeast face of the model is normal to the strike of the fracture zones as seen in the area of the excavations. The geology of this face is shown. Fracture Zone 2 has a sharply arcuate outcrop pattern along the south and west side of the model. The overlying rock block is "split" by Fracture Zone 3 and Fracture Zone 2.5, both of which curve and merge with Fracture Zone 2 to the south.

The orientation of the present-day maximum principal in situ stress, relative to this model, is shown in Figure 12. Two distinct stress domains have been recognized. In the sparsely fractured rock below Fracture Zone 2, the maximum horizontal stress is oriented NW-SE, perpendicular to the strike of the thrust fault. In the block above Fracture Zone 2, the maximum principal stress is considerably lower and is oriented NE-SW, parallel to the dominant fracture set and the strike of Fracture Zone 2. This presumably represents a reduction and re-orientation of stresses through the formation of fractures in the hangingwall block. These stresses were apparently not relieved in the footwall.

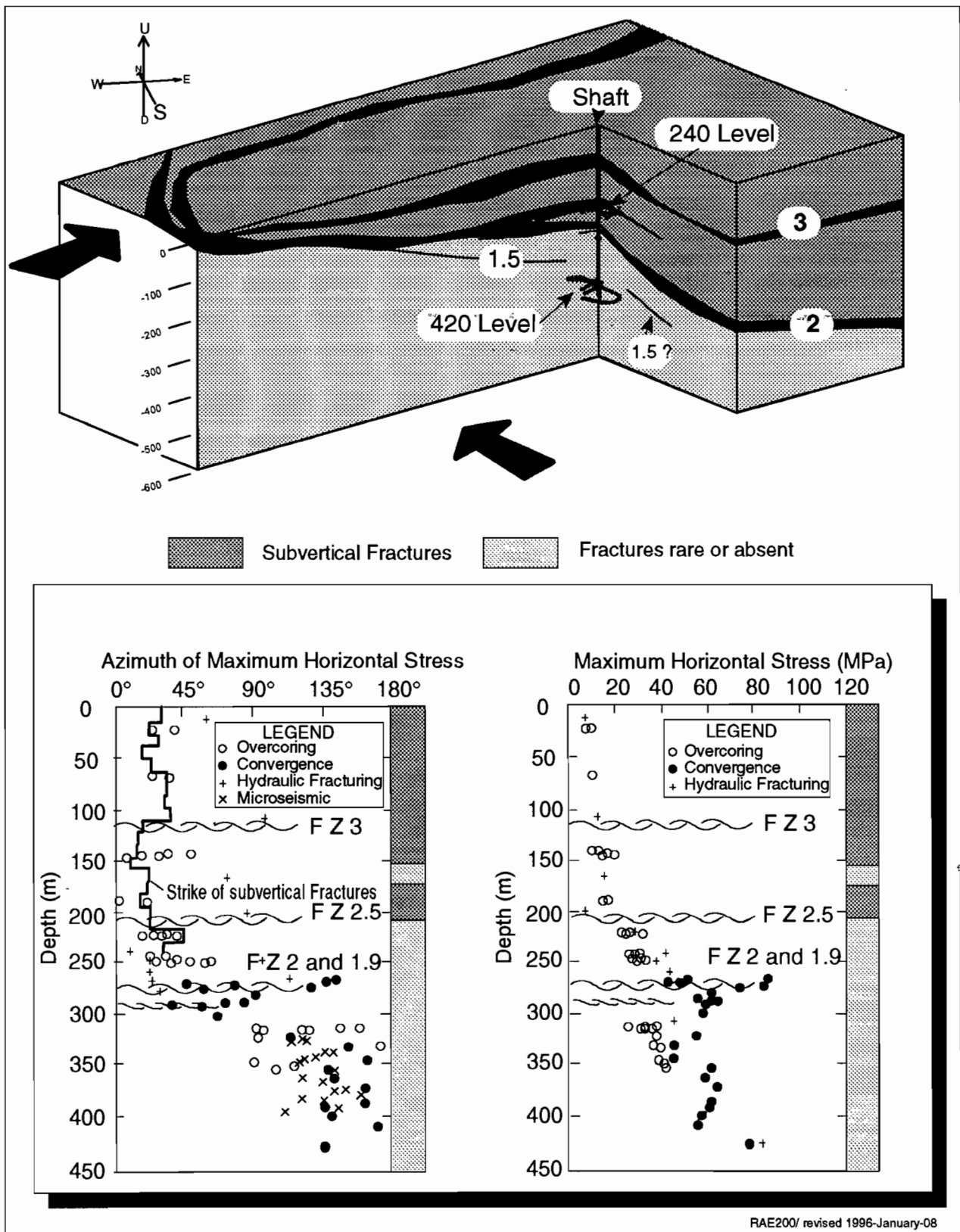


Figure 12. In situ stress domains in the URL in relation to the fracture domains (stress data from Martin 1989).

The geometry of the thrust faults suggests they were formed when the regional stress field was oriented such that the plane containing the maximum and intermediate principal stresses was subhorizontal, with the former aligned in the NW-SE direction. This deformational event is believed to be associated with plate accretion on the margins of the Superior craton during the late Archean - early Proterozoic (Ayres 1978; Card and Ciesielski 1986). The present in situ stresses at depth (420 Level) in the URL retain this geometry, which supports the suggestion by Haimson (1990) for a domain in the mid-continent region in which the maximum horizontal principal stress is directed NW-SE.

In the case of Fracture Zone 2, the simple conjugate system of fractures suggests that strain accommodated by fracturing was largely two-dimensional. In the case of Fracture Zones 2.5 and 3, however, the orthorhombic pattern of low-dipping major and minor fractures suggests that brittle strain was three-dimensional (Davis, 1984). This difference is seen as a consequence of Fracture Zones 2.5 and 3 being "piggybacked" on Fracture Zone 2, which has had the major movement. As such, the more complex displacements (strike, oblique, and reverse dip-slip) in Fracture Zones 2.5 and 3 probably represent a natural accommodation to displacement on the underlying and dominant thrust fault (Fracture Zone 2).

The subvertical fracture sets are interpreted as extensional intrablock fracturing initiated by geometric flexing and general expansion of the thrust plates, probably in the early Proterozoic. The plane containing the maximum and intermediate principal stresses was still subhorizontal, but the local maximum principal stress axis was now aligned NE-SW. Reactivation and extension of some fractures must have occurred during Paleozoic transgression, during subsequent removal of the Paleozoic cover, and during continental glaciation. This is supported by the various ages of infillings in these sets (Table 1).

The decreasing frequency, extent and complexity of subvertical fracturing with depth from surface are seen as a consequence of both the stacking of the thrust plates, and of the distance from surface. The greatest and most varied "flexing" and fracturing would be suffered by the uppermost blocks. Within a single fracture domain, the pattern and frequency of subvertical fracturing reflects the distance from, and configuration of, the underlying thrust fault. In fracture domain "B" (the area of the 240 Level) for example, the pattern of subvertical fractures varies from unimodal to bimodal (orthogonal) as the wedge of rock between Fracture Zone 2 and Fracture Zone 2.5 thins out to the south. Similar variations are seen in the complexity and preferred orientations of fracturing in Fracture Domain "A", as the plane of Fracture Zone 3 curves from NE- to N-striking.

Hydrogeology

Prior to construction of the URL, the natural, undisturbed hydrogeological conditions at the site were characterized by small-scale tests on individual boreholes, large-scale multiple-borehole hydraulic interference tests, and groundwater sampling for aqueous geochemistry. Several types of multiple-interval completion systems were installed in the boreholes to measure the hydrogeological conditions within the rock mass, and a program of both automated and manual monitoring was implemented to

establish baseline piezometric conditions. These investigations revealed that the three major, shallow-dipping fracture zones (FZ1, FZ2, FZ3) largely control the patterns of groundwater movement and groundwater chemistry within the rock mass at the URL site (Figure 13). The hydrogeological conditions of Fracture Zones 2 and 3 have been determined in considerable detail using a variety of borehole testing techniques such as straddle packer tests and large-scale multiple-borehole hydraulic pressure interference tests. The results of the testing revealed a complex spatial pattern of permeability within each of the fracture zones which strongly controlled the patterns of both groundwater movement and chemistry. Permeability of unfractured rock in the batholith generally decreases with depth, such that the permeability of unfractured rock below about 700 m depth does not exceed 10^{-12} m/s (Davison et al. 1994).

The baseline investigations were used to develop and to calibrate various numerical computer models to describe the 3-dimensional hydrogeology of the site. These models then were used to predict the piezometric drawdown that would develop in the rock mass during and after the first stage of excavation of the URL shaft, to a depth of 255 metres, and the modelled predictions were documented prior to the start of excavation. The shaft was located such that it passed through Fracture Zone 3 and an upper low-permeability limb of Fracture Zone 2, but it avoided the main high-permeability portion of Fracture Zone 2. The time-variant rate of groundwater inflow to

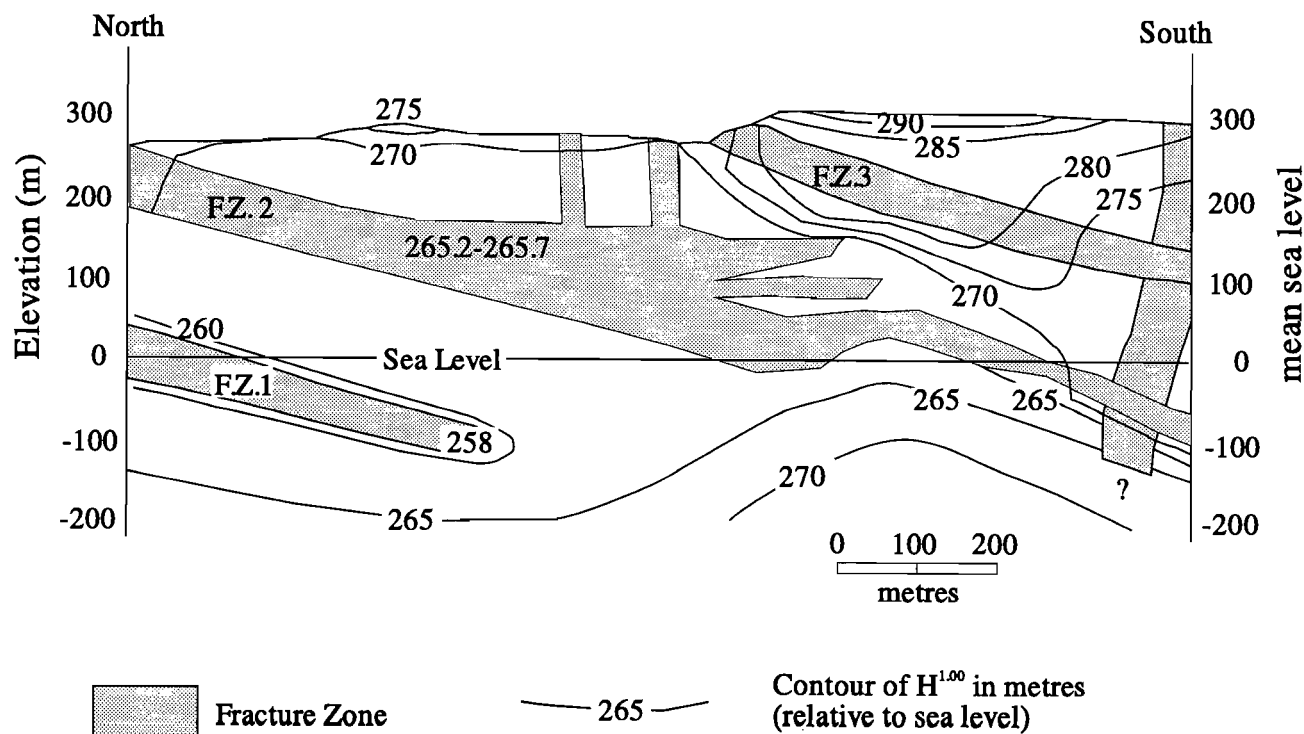


Figure 13. Characteristic hydraulic pressure conditions as measured prior to excavation (after Davison 1982). Pressures are expressed as equivalent fresh water elevation head ($H^{1.00}$) to account for variations in groundwater chemistry between the fracture zones.

the shaft excavation was also predicted. As expected, most drawdown occurred within Fracture Zone 3 and in a network of NNE-trending subvertical fractures extending about 80 m above and below Fracture Zone 3. Very little drawdown developed in Fracture Zone 2, also in accordance with the modelled predictions.

Hydrogeological experiments in the URL have continued to study the extreme variability in the hydraulic characteristics of the fracture zones, and are used to develop and test detailed models that simulate groundwater movement through rock and through excavation damage around tunnels. Among other studies, travel time and the recharge path of groundwater flow in the granite have been modelled; the results compared well with groundwater residence times estimated from $^2\text{H}/^{18}\text{O}$ data from the URL area (Gascoyne and Chan 1992).

Groundwater geochemistry

The groundwater salinity (i.e., total dissolved solids, TDS) in the Lac du Bonnet Batholith, like that of many other localities on the Canadian Shield (Frape et al. 1984), generally increases with depth (Gascoyne et al 1987). Variation in TDS and chlorinity with depth in the vicinity of the URL site show that high TDS concentrations in shallow groundwaters, due to bicarbonate and sulfate derived from overburden materials, decrease in the subsurface to a depth of about 300 m, then increase exponentially with linear increase in depth (Figure 14a). In contrast, groundwater chlorinity (Figure 14b) shows a steep, continuous increase throughout the depths sampled. In both cases, a reduction of slope occurs at a depth of between about 300 and 400 m; the rate of increase in TDS and Cl below this depth is reasonably constant. Measurements of ^{36}Cl in the groundwaters and in rock matrix solutions suggest that the groundwater salinity is largely derived from dissolution of soluble salts in the host rock (Gascoyne et al. 1994).

Shallow bedrock groundwaters in the region are generally Na-Ca-(HCO_3) dominated. With depth, Ca, Na, and Cl increase and eventually account for more than 90% of the TDS. The transition in chemistry from shallow to deep groundwater is also marked by decreased concentrations of HCO_3 . Complex mixing of deep saline waters and near-surface recharge waters takes place in the fracture zones (Figure 15), and continued interaction with the host rock causes near-surface discharging groundwater to be quite saline.

Concentrations of natural U in groundwater are high in the upper 100-200 m of the Lac du Bonnet Batholith, attaining concentrations of almost 1 mg/L in both overburden and bedrock water samples (Gascoyne 1989). Much lower U concentrations (less than 30 $\mu\text{g/L}$) are present below this depth range. The key control on U concentration in these waters appears to be redox potential. Gascoyne and Barber (1992) attributed the changes with depth to a combination of lower Eh groundwater and reduced availability of bicarbonate at depth to form soluble anionic U complexes. In contrast to U, concentrations of natural Ra increase at depth. The increase may be caused by a reduction in the availability of sorption sites at high salinities at depth. The Ra enrichment also may be the result of direct dissolution of alpha-recoiled Ra from U-rich fracture linings, where U became less soluble and precipitated on surfaces in the deeper fractures.

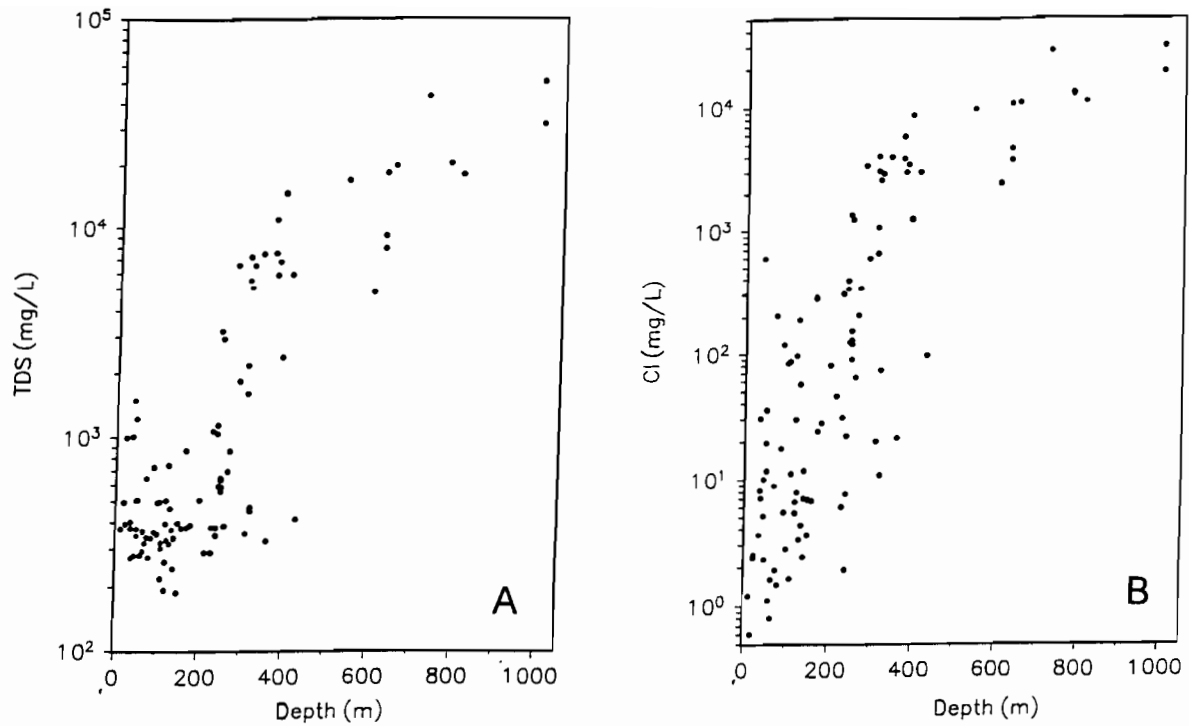


Figure 14. Variation in WRA groundwater chemistry with depth for: (A) total dissolved solids (TDS) and (B) chlorinity.

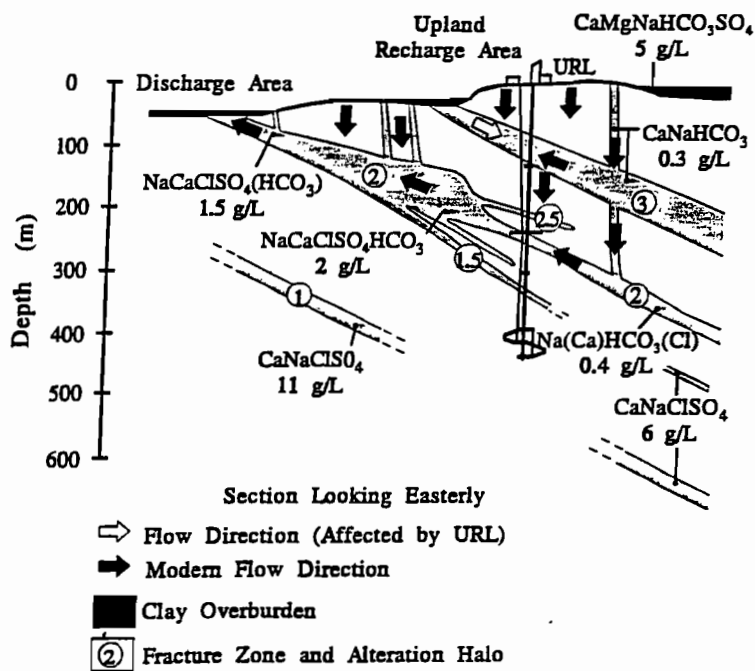


Figure 15. Schematic representation of groundwater compositions at the URL lease site, showing groundwater flow paths and geochemical patterns in fracture zones.

DESCRIPTION OF FIELD TRIP STOPS

For logistical reasons, all stops on this one-day field trip are limited to outcrops and excavations on the URL lease site, and most of the day will be spent underground. The trip will emphasize the lithology of the equigranular to porphyritic biotite-bearing granite which is the main rock type of the Lac du Bonnet Batholith, and the correlations between litho-structural, hydrogeological, and in situ stress domains. The main features to be observed are:

- large-scale compositional layering in granite
- transition from roof zone to batholith interior
- transition from fractured and altered rock at surface to intact or sparsely fractured pristine rock at depth
- influence of lithology on the fracture system
- relationship between subvertical fractures and the thrust faults and splays

The URL is located 14 km east of the town of Lac du Bonnet, which is about 130 km northeast of Winnipeg (Figure 2). From Highway 11 at Lac du Bonnet, drive east on Provincial Road 313 for 12 km to Belluk Road (which is about 0.5 km past the Pinawa Channel bridge). Turn right and proceed south on this gravel road for 1.6 km to the entrance gate to the URL lease site. Turn left through the URL gate and proceed up the hill to the URL parking area.

The URL is open for public tours at no charge year-round on Fridays at 10:00 a.m. and 1:30 p.m. Reservations are required by calling Whiteshell Laboratories at 1-800-665-0436.

Stop 1. Overview from hillside NW of URL parking lot.

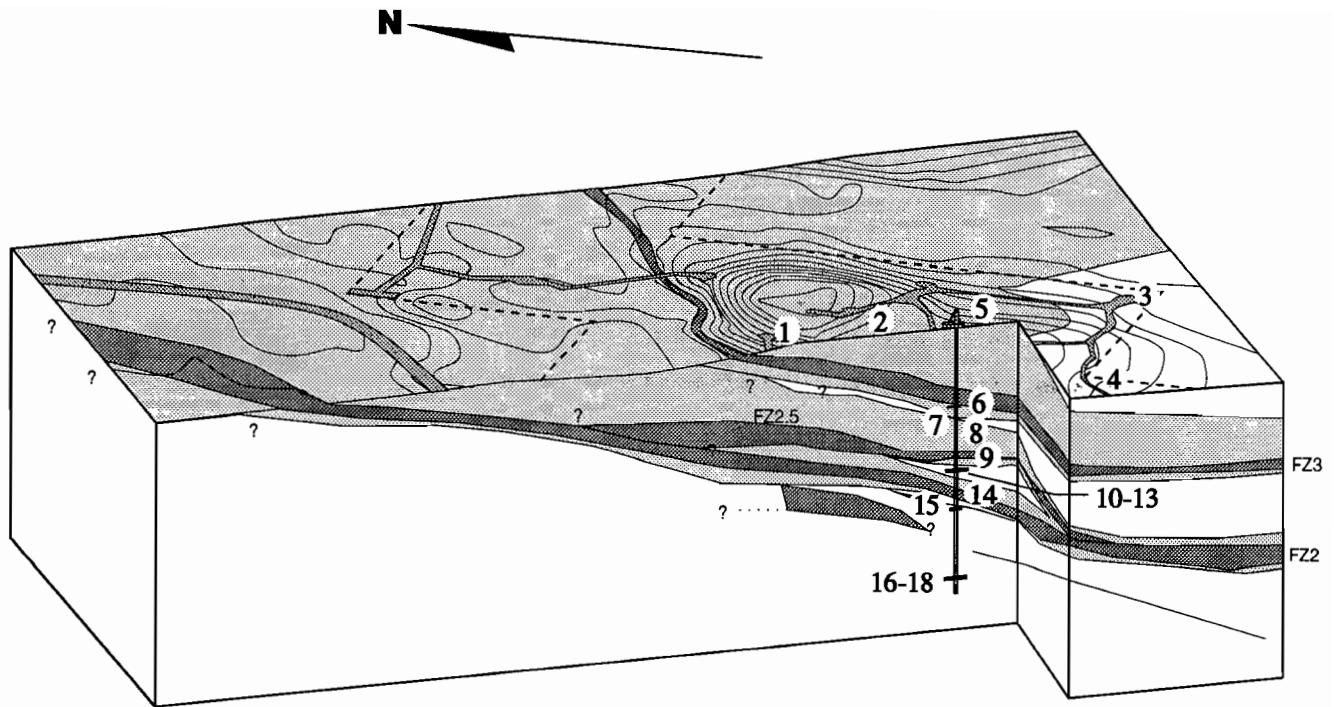
This stop provides an overview of the surface facilities at the URL and an orientation of surface topography relative to the major structural elements in the subsurface (Figure 16).

After the initial overview (Stop 1), the field trip will focus sequentially on:

- Stops 2 - 9 Features of the roof zone
- Stops 10 -13 The transition from altered and sparsely fractured rock to unaltered and largely intact rock
- Stops 14-18 The sparsely fractured main phase of the granite, high in situ stresses, and extensive granodiorite dike swarm exposed in the batholith interior.

As time permits and depending on accessibility, it may also be possible to view:

- ongoing experiments to design and test various components of the multi-barrier geological disposal concept,
- the results of efforts to reduce excavation damage through progressive improvements in excavation design and construction methods, and
- the correlations between lithology, fractures, in situ stresses, hydrogeology and excavation damage which are applicable to the general problem of site selection and investigation.



Tour Stops

1-5	Surface	10-13	240 Level
6	130 Level	14	Shaft (FZ 2.0)
7	Shaft	15	300 Level
8	Shaft	16-18	420 Level
9	Shaft (FZ 2.5)		

Figure 16. Panoramic view (Stop 1) showing the relationship between surface topography, the fault zone outcrop, and geology at the URL. The location of the trip stops relative to the major structural features on site is also shown.

Stop 2. Fractured xenolithic granite in thrust fault (FZ3) hangingwall

Fracture Zone 3, the uppermost of the low-dipping thrust faults in this area, sub-crops beneath the overburden at the base of the escarpment at this stop and has been traced downdip through its intersection with the URL shaft (Figure 16). The exposures consist of schlieric or layered granite with numerous mafic enclaves, many of which are entrained in a felsic matrix of coarse to very coarse-grained segregations of apparently late-stage differentiates. Individual xenolithic horizons, compositionally distinct, are areally extensive and have been traced from surface downdip to the URL through multiple borehole intersections.

An extensive network of fractures is present in the lower 100m of the hanging-wall block of the fault. At least three subvertical sets are present in addition to low-dipping sets. Some of the low-dipping fractures are related to surface relief, while

others, with lower greenschist facies infilling assemblages, are older and are thought to be genetically and geometrically related to events late in the crystallization of the roof zone or to the development of the low-dipping faults. Shaft mapping reveals that the subvertical fractures are truncated by the low-dipping shear fractures within Fracture Zone 3. Faults and subvertical fractures tend to be preferentially developed at the margins of the xenolithic granite. To the southeast, over the crest of the ridge, the granite becomes increasingly homogeneous (stops 3,4), and fracture frequency is substantially reduced.

STOP 3: Moderately fractured granite, epidote-filled fractures, and surface exposure of the tip of the granodiorite dyke swarm. .

In a structural sense, this outcrop is located about 150 m above the thrust fault (Fracture Zone 3), and it overlies the xenolithic granite of the previous stop. Features to note at this location include:

- fewer fractures and less alteration in general compared to previous outcrops
- increased homogeneity of granite compared to the previous outcrops
- epidote-filled subvertical fractures and localized alteration in granite
- surface exposure of the granodiorite dyke

This is an example of moderately fractured rock at the URL (i.e., one or two fracture sets, spaced 1-5 m apart). Several of the fractures exposed at this outcrop contain epidote, which is relatively uncommon in the fracture mineral assemblage for the batholith. Other stops in the field trip will show examples of highly fractured and sparsely fractured rock. Surface exposures of the granodiorite dyke swarm, as typified by this outcrop, are rare. The dyke swarm is much better developed at depth; good exposures of well-defined, fine-grained granodioritic to granitic dykes will be viewed underground later in the field trip.

STOP 4: Sparsely fractured granite, pegmatite dykes, strain measurements.

During URL site characterization, this locality was used for recoverable strain measurements (Figure 17). Structurally, this outcrop is approximately 170 m above the top of the thrust fault Fracture Zone 3. The subvertical fractures seen at the last stop are absent, and the rock is unaltered. Features of interest include:

- decrease in alteration and frequency of fractures over the general outcrop area compared to the previous stops,
- textural homogeneity of the granite at this location, and
- sheared pegmatite dykes with dilational, quartz-filled step-outs.

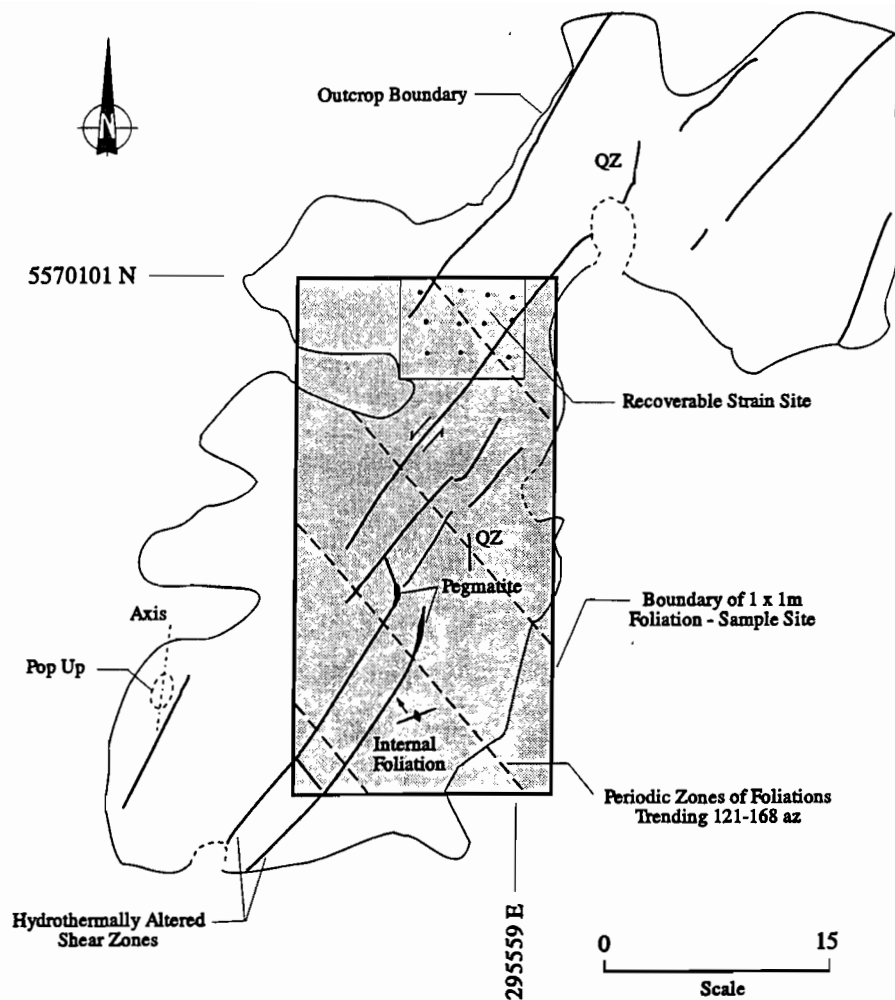


Figure 17. Outcrop of sheared fine-grained granite zones, with left lateral strike-slip movement and pegmatitic terminations (Stop 4). The outcrop was also the location for recoverable strain measurements

STOP 5: URL headframe

At this point, participants will proceed underground for the remainder of the field trip. Boots, hard hats, coveralls, and accessory lights will be provided at the URL for all participants. Depending on the total number attending, participants may be split into two groups for transport in the hoist and for viewing stops at the 240 and 420 Levels. In such an event, not all stops will be visited in consecutive order.

STOP 6: (Optional) Fracture Zone 3 in the URL shaft, 120 m depth

This exposure of Fracture Zone 3, the uppermost major thrust fault, is located in the access shaft at a depth of 120 m. Access to this site is limited under normal circumstances, and will be at the discretion of Site Operations. All visitors must remain in the cage. Features to note here include:

- large-scale control of fractures by litho-structural domains
- small-scale control of fracturing by foliation in the granite
- overall appearance of fault zone, including basal cataclasite zone and chloritic splays in the hangingwall block
- subvertical intra-block fracturing in both the footwall and hangingwall.

At this location, Fracture Zone 3 straddles the contact between a gneissic granite domain and a xenolithic granite (Figure 18). This correlation between lithological contacts and fault location has been traced through multiple borehole intersections and extends over an area of at least 1 km². In and near the exposure of the fracture zone in the shaft, the compositional layering and the faulting have an average orientation of about 058°/16° SE. However, many individual fractures parallel the local-scale gneissic and schlieric banding. This implies that where the local fabric approximately coincides with the theoretical failure plane for fault formation, the fracturing follows the orientation of the local, small-scale heterogeneities. This is most obvious in the hangingwall above the basal cataclastic zone, where the average fracture and foliation attitudes are 029°/26° SE and 030°/30°, respectively.

The upper boundary of Fracture Zone 3 is marked by a single chloritic fracture oriented 030°/30° SE and by a narrow zone of secondary fracturing and alteration. A pegmatite dike and a quartz vein show reverse dip slip displacement, with an apparent offset of 4 cm.

The base of the fault zone is more complex, consisting of a braided shear zone about 1 m in width, with complexly fractured and altered rock blocks bounded and segmented by chloritic slip surfaces and a cataclastic matrix. The cataclasites consist of recrystallized fault rubble cemented by a fine grained chlorite-carbonate matrix. They are crosscut by the chloritic slip surfaces, minor fractures, and seams of soft clay - goethite gouge. This assemblage is in varying degrees of groundwater-induced decomposition. Parallel and antithetic fractures occur throughout the hangingwall, and to a lesser extent in the footwall.

Fracture Zone 3 is more structurally varied and complex than the deeper fracture zones. There is a greater scatter to the orientations of all fracture sets in this zone compared to the others, and there are two additional low-dipping fracture sets that are not found in the deeper faults. In Fracture Zones 2 and 2.5, subvertical fractures have propagated from the cataclasite zone upwards into the overlying block. In Fracture Zone 3, subvertical fractures extend into the footwall as well as the hangingwall. This greater complexity and degree of fracturing is believed to be a consequence of the relative position of Fracture Zone 3 at the top of the thrust pile. In other respects, however, Fracture Zone 3 resembles the deeper fracture zones. These similarities include:

- a broad zone in the hangingwall with large low-dipping chloritic shear fractures (splays) and subsidiary fractures. The abundance and variety of infillings in these subsidiary fractures is greatest at their intersection with the fault zone, and decreases with distance,
- a cataclasite horizon and major slip surfaces with offset at the base of each fault, and

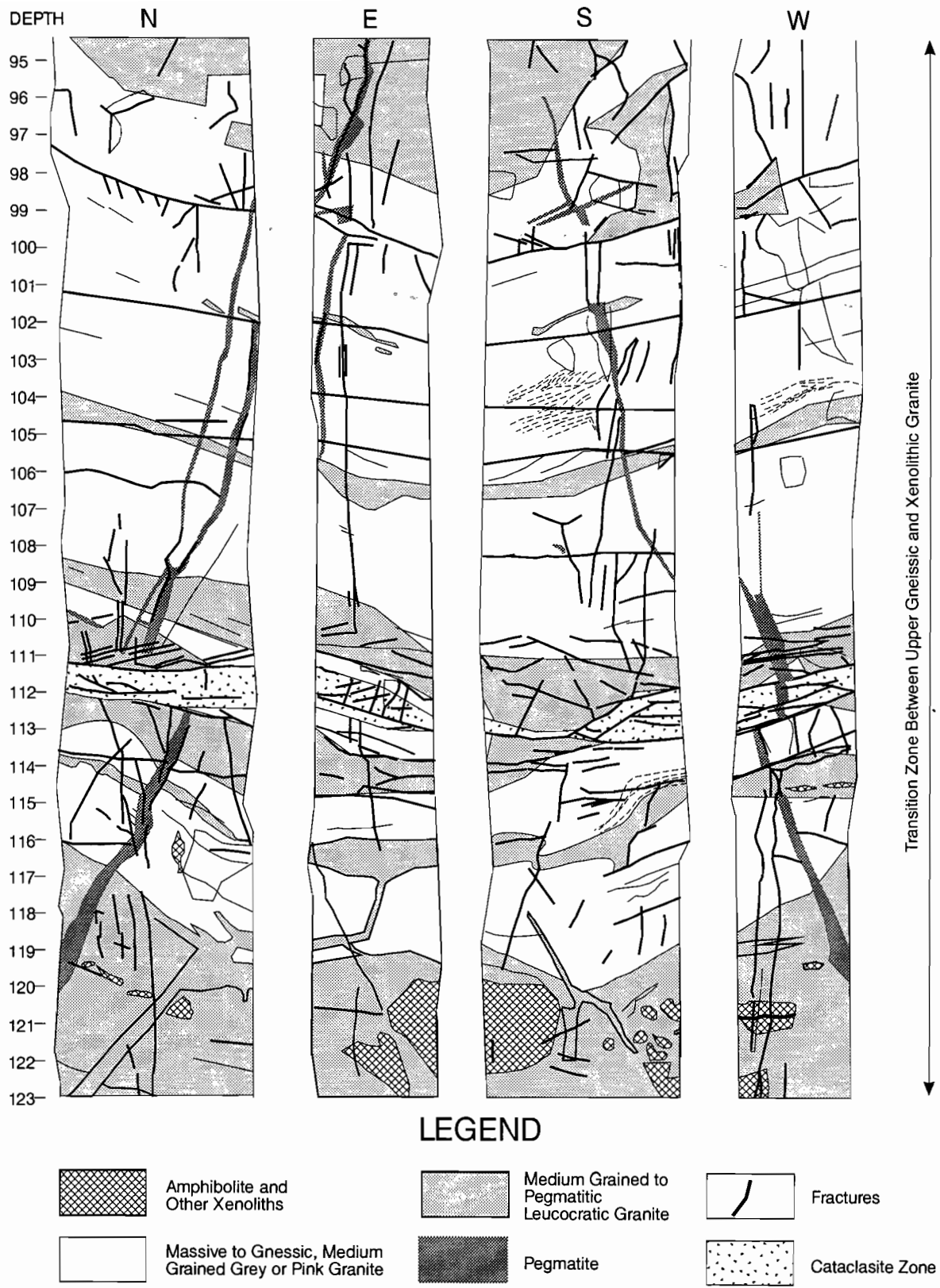


Figure 18. Simplified geological map of the shaft walls at Fracture Zone 3 (Stop 6).

- an encompassing alteration halo in which the granite is changed from grey or pink to red brown or cream. (The dimensions of the altered and fractured regions in the footwall and hangingwall of this fault, and of the other faults, are quite variable but generally decrease with decreasing fracture permeability.)

Like the other faults, Fracture Zone 3 is a boundary separating rock blocks with differences in fracture density and pattern, and with different in situ stress orientations and magnitudes. This last point is demonstrated by the changes in orientation of the stress-induced fractures across the fault.

STOP 7: Xenolithic granite and subvertical fractures at the 130 Level

The 130 Level Shaft Station is one of two access stations apart from the main testing levels in the shaft (Figure 4). The granite exposed at this stop is pink to red in colour, coarse-grained to pegmatitic, and contains abundant xenoliths in a range of sizes up to 10 m in length. Most of the xenoliths are metavolcanic and include amphibolitic, quartz-pyrite-chloritic, and carbonate-bearing examples.

The 130 Level Shaft Station is about 15 m below the base of Fracture Zone 3 and so is within Fracture Domain "B", which extends from the base of Fracture Zone 3 to the base of Fracture Zone 2.5. Subvertical fractures are largely confined to the margins of this domain, in its upper and lower thirds. The geometric pattern of fracturing is simpler and more ordered than that seen above Fracture Zone 3. A single NE-striking subvertical fracture set predominates, one example of which is visible at this stop. The spacing in this fracture set is zonal, varying from one xenolith to the next. Infillings include hematite and carbonate. Chlorite is preferentially developed in the portions of the fracture within and below the xenoliths.

STOP 8: (Optional) Litho-structural domains in the shaft, 150m depth.

Access to this stop, at 150 m depth in the shaft, is limited under normal circumstances, and may be restricted at the discretion of Site Operations. All visitors must remain in the cage.

This stop examines the contacts and the differences in deformation between three litho-structural domains at depths between 150 m and 170 m in the shaft (Figure 19). The domains consist of an upper and a lower xenolithic granite, separated by a domain of massive to weakly gneissic granite.

The two xenolithic domains consist of amphibolitic and metavolcanic xenoliths in a coarse-grained to pegmatitic granite matrix, with abundant flow banding and biotitic schlieren. A number of features at this locality suggest differential movement and mingling of incompletely solidified components of the batholith roof zone, with the gneissic granite at this location behaving more rigidly than the xenolithic granite:

- A fold in the flow banding of the upper xenolithic granite is abruptly truncated against the contact with the massive to weakly gneissic granite.
- Compositional layering in the gneissic granite, 5 m from this contact, displays boudinage structure

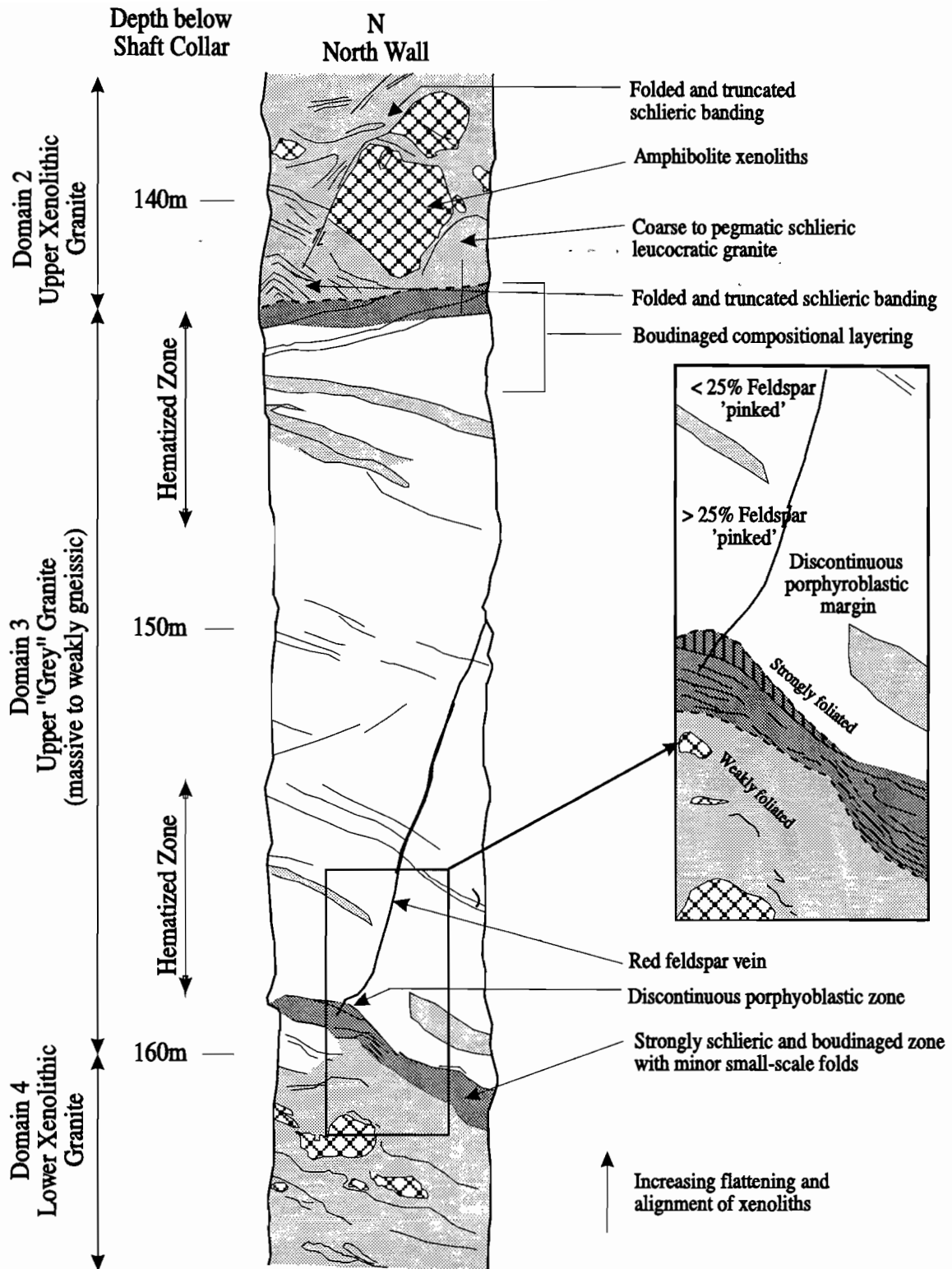


Figure 19. Simplified geological map of 3 litho-structural domains in the URL shaft between 135 and 170 m depth (Stop 8).

- Xenoliths, particularly those in the lower domain, are strongly flattened within 5 m of the contact, whereas xenoliths at a greater distance are undeformed.
- Undeformed xenoliths adjacent to the gneissic granite tend to have their long axes aligned parallel to the contact, but xenoliths further from the contact are more randomly oriented.
- A pegmatitic lens with very coarse microcline porphyroblasts occurs against the lower contact of the gneissic granite, and some of this material intrudes several metres into the gneissic granite.

Drilling from the 130 Level Shaft Station has shown that the gneissic granite thins rapidly and terminates 20 m up-dip, and a similar distance to the southwest along strike.

This stop also illustrates the transition from moderately to sparsely fractured rock in the centre of Fracture Domain B. The NE-striking subvertical fractures that characterize Fracture Domain B are largely limited to the xenolithic granite. The gneissic granite is for the most part unfractured and unaltered.

STOP 9: Fracture Zone 2.5 in the shaft, 215 m depth.

Access to this stop, at 215 m depth in the shaft, is limited under normal circumstances, and may be restricted at the discretion of Site Operations. All visitors must remain in the cage. Noteworthy points at this stop include:

- large -scale control of fracture zone location by litho-structural domains
- local-scale control of fracturing by foliation in the granite
- fault structure, including basal slip cataclasite zone, chloritic splays in the hangingwall block, and
- subvertical intra-block fracturing in the hangingwall only, and the termination of the subverticals at the base of the fault zone.

Fracture Zone 2.5 is a wedge-shaped splay with little apparent offset that branches from the top of Fracture Zone 2. It is intersected by the shaft between depths of 202 to 217 m, but it terminates less than 50 m from this location. The local orientation of Fracture Zone 2.5 here (WNW strike, SW dip) is markedly different from Fracture Zones 2 and 3 (NE strike, SE dip). This difference may be attributed, at least in part, to control by earlier rock structure. Fracture Zone 2.5 follows the contact between litho-structural domains 5 and 6 (two gneissic granites), over an area of about 200m², based on data from multiple borehole intersections and the vent raise. Fabric control at the outcrop scale is most obvious at the base of the fault, where prominent anastomosing chloritic slip surfaces follow biotitic schlieren bands.

There are few markers, but offset sense and displacement across Fracture Zone 2.5 appear to be very minor. A maximum of 10 cm of reverse dip-slip displacement has been observed on the basal chloritic fracture of this zone, with no visible offset on any of the other low-dipping fractures throughout the overlying 20 m of the hangingwall fractures. Cataclasite has been found in this fault by boreholes drilled to the southwest of the shaft, but the absence of a cataclastic horizon at this stop is consistent with negligible offset across the fracture zone. Slickenlines on the large, low-dipping, sub-

horizontal fractures indicate dip-slip movement, with an oblique component for the NW-striking low-dipping fractures. Vertical fractures display horizontal and subvertical lineations.

The most noteworthy feature of Fracture Zone 2.5 at this locality is its effect on the distribution and extent of subvertical fractures (Figure 20). In the hangingwall above Fracture Zone 2.5, one set of NE-striking subvertical fractures is abundant. The number of fractures in this set increases with proximity to the base of Fracture Zone 2.5, and the variety and amount of infillings within each fracture also increase. This subvertical fracture set is abruptly terminated at the base of Fracture Zone 2.5. The footwall block, which is exposed in the shaft raise, at the 240 Level, and in an extensive array of boreholes, is virtually fracture-free, with fractures restricted to minor rock types (such as dykes), or to the margins of the fault zones (as described in the next stop).

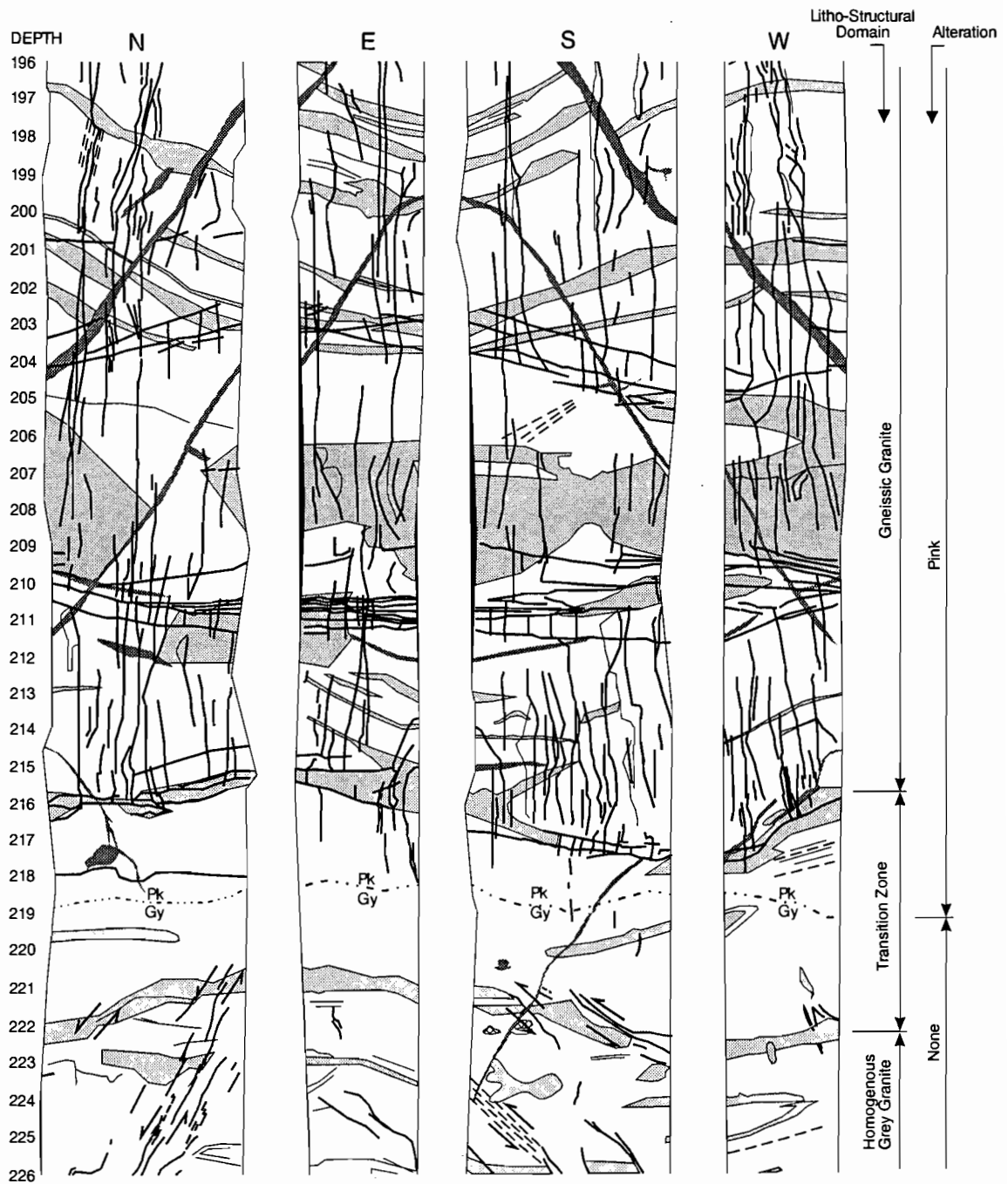
STOP 10: 240 Level Station: Geology of the 240 Level

The uppermost of the two main levels, the 240 Level is the site of many URL experiments. The arrangement of tunnels in the 240 Level is roughly pentagonal in plan view, with rooms for experiments branching from the sides and ends of the tunnels (Figure 4). Construction of the 240 Level involved the development and testing of a number of engineering techniques to reduce excavation damage through improved excavation design and execution. The success of these techniques, aided by relatively low stresses in the rock at this depth, is illustrated by the smooth walls and high percentage of perimeter blast hole tracers (half-barrels) remaining on the excavation surfaces throughout most of the 240 Level.

Structurally, the 240 Level is situated within an open-ended wedge-shaped block, the margins of which are defined by the upper and lower surfaces of Fracture Zones 2 and 2.5, respectively (Figure 21). Fracture Zone 2.5 pinches-out approximately 65 m to the east of the shaft and merges with the top of Fracture Zone 2 approximately 80 m to the northwest. The gross scale permeability of Fracture Zone 2 increases to the northwest, apparently due to its intersection with Fracture Zone 2.5, and to the increasing frequency and complexity of fracturing between them. The transition between fractured ground to the west and largely intact ground to the east is coincident with a grey (unaltered) and pink (altered) colour boundary in the granite (Figure 22).

The batholith at this depth is medium grained and variably gneissic. It is host to a variety of leucocratic segregations and metasomatized zones, most of which occur as irregular lenses or sills concordant to the surrounding gneissosity. Amphibolitic or tonalitic xenoliths may occur in association with these leucocratic zones but are generally rare at the 240 Level.

Fractures exposed within the excavations and boreholes of the 240 Level are NE-striking and subvertical. They occur either as major joint zones extending tens of metres vertically and horizontally, or as non-persistent fractures confined either to the granodiorite dykes or to the early granitoid (coarse granite to pegmatite) sills (Figure 22). The major joint zones truncate against the thrust faults, and are water-bearing.



LEGEND

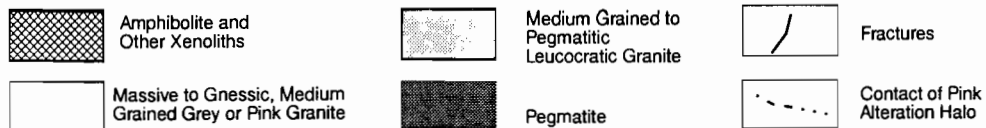
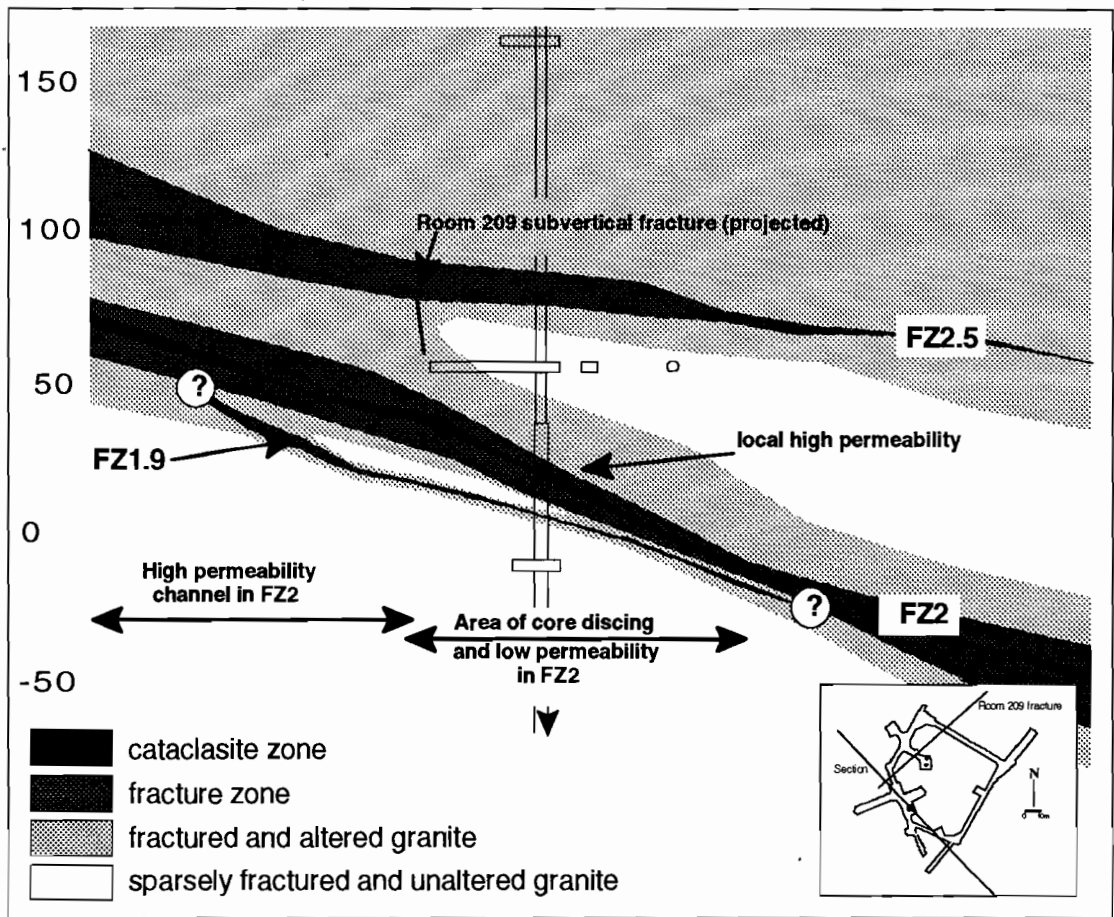


Figure 20. Simplified geological map of the shaft walls at Fracture Zone 2.5 (Stop 9).



USA9306/ R.A. Everitt/ 1994-Feb-25

Figure 21. Simplified geological cross section through the 240 Level, here indicated by Room 209, showing its location relative to Fracture Zones 2 and 2.5 (Stop 10).

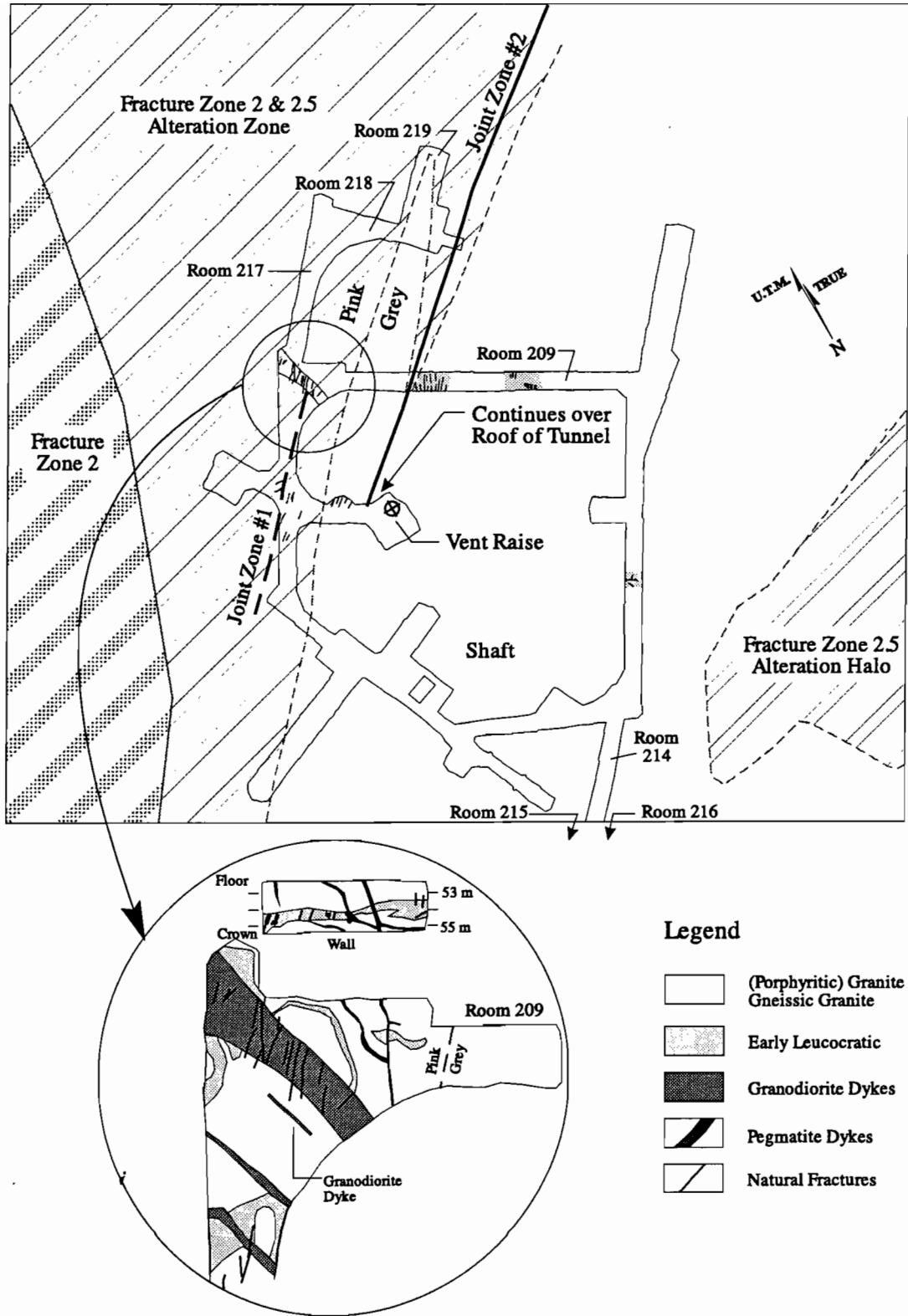


Figure 22. Simplified geological map of the 240 Level showing the type and locations of fractures.

The following features will be examined at various locations on the 240 Level:

- transition from fractured and altered rock to unfractured and unaltered rock
- granodiorite dykes
- several generations of late auto-intrusive pegmatites / granites
- outcrop-scale control of fracture distribution by lithology
- efforts to reduce excavation damage through improved excavation design and execution.

STOP 11: (Optional) Transition from fractured to unfractured granite near Fracture Zone 2.5 (Solute Transport for Moderately Fractured Rock Experiment)

The Solute Transport in Moderately Fractured Rock Experiment (MFR) was designed to determine hydrogeological and chemical transport properties in a large volume (10^5 m^3) of rock that has, on average, 1-5 fractures per metre on a line sample (Simmons et al. 1992). The access tunnel (Room 214), and the drilling station tunnels (Rooms 215 and 216) for this experiment expose a section through the alteration halo underlying Fracture Zone 2.5 in which the transition can be observed from unaltered and unfractured rock to altered and locally fractured rock (Figure 23).

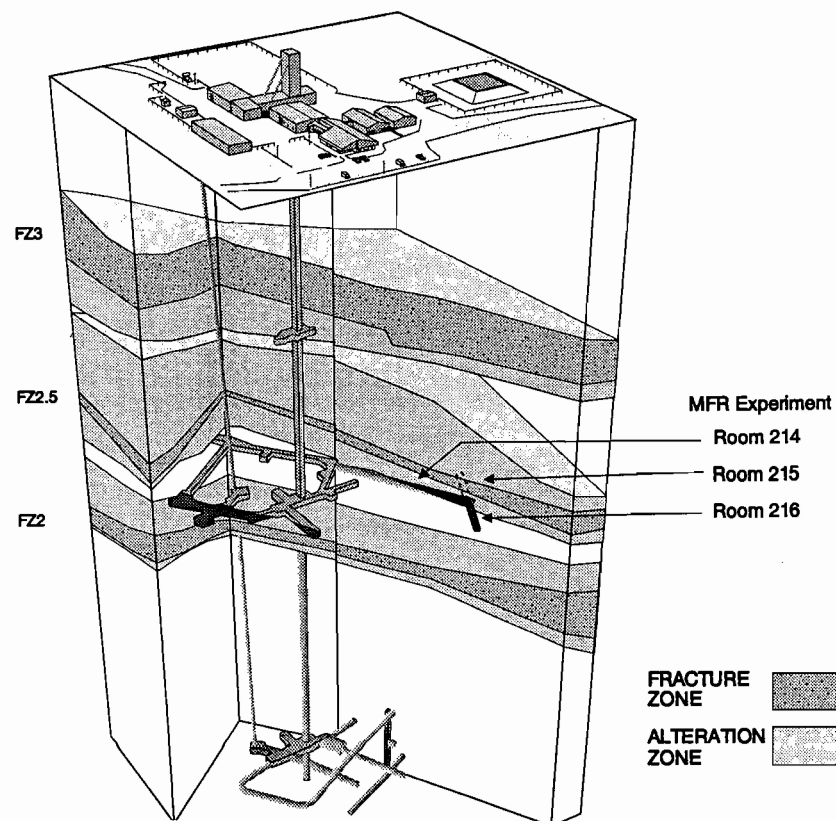


Figure 23. Location of fracture zones and alteration haloes in relation to the access tunnels for the MFR Experiment (Stop 11).

The main rock unit in the MFR tunnels is a compositionally and texturally banded, grey to pink gneissic granite. It is host to three auto-intrusive phases:

- early fine-grained to pegmatitic leucogranite segregations
- granodiorite dyke swarm
- late pegmatite dykes

The early leucocratic segregations are largely confined to an irregular layer about 2 m to 2.5 m thick which strikes northeasterly and dips along the gneissosity (about 25°NE). This heterogeneous layer is significant as it hosts nearly all of the sub-vertical fractures seen in the MFR excavations.

A single metre-wide granodiorite dyke occurs at the junction of Rooms 215 and 216. Related small dykes and ductile shear zones are distributed throughout Room 215, where they comprise biotitic quartzo-feldspathic bands that offset and deform earlier layering. The main dyke has an average orientation of 128°(218°)/47°, and it is strongly flow banded.

The pegmatite dykes are uniformly distributed in all rock types present at the 240 Level. This is in contrast to the 420 Level, where pegmatite dykes are limited to the interior of the granodiorite dyke swarm. The subvertical pegmatite dykes are hydro-geologically significant because local parting along the dyke contacts has produced open fractures.

At the URL, the frequency and complexity of fractures increases with proximity to the fault zones. This pattern is apparent through the cross section provided by the tunnels. The access tunnel (Room 214) is in unfractured and unaltered granite, but the entire drill station area (Room 215-216) is within the pink alteration halo underlying Fracture Zone 2.5. For any given rock type, colour grades from brick red near the crown to light pink or grey in the floor. The alteration halo marks the extent of micro- to outcrop-scale fractured rock beneath Fracture Zone 2.5. The process of “pinking” occurs by deposition of hematite along grain boundaries and microcracks, and is clearly evident in the coarser-textured units. The secondary nature of the pink / grey alteration halo (associated with Fracture Zone 2.5 above the tunnel) is clearly evident as it is superimposed across the dyke contact. Four sets of fractures are recognized on the basis of orientation and mode of occurrence:

- NE-striking subvertical fractures confined to the early leucocratic segregations, trace length less than 0.75m, with hematite infilling.
- NW-striking subvertical fractures confined to the early leucocratic segregations, hematite infilling.
- one throughgoing NNW-striking subvertical fracture with hematite infillings, exposed on the northeast wall of Room 215. This fracture is not confined by lithology.
- one low-dipping fracture confined to a very prominent biotitic band (old ductile shear zone). There is partial alteration of the biotite to chlorite along the fracture, and lineations plunge along the dip-direction of its surface. As such, this fracture is similar in geometry, mode of occurrence and appearance to those which comprise the URL fracture zones. The extent of the fracture beyond the tunnel is unknown at this time.

STOP 12: Correlation between fractures, in situ stresses, and hydraulic transmissivity at the 240 Level

Hydraulic studies in the URL before, during, and after shaft construction have revealed complex local and regional scale patterns of transmissivity within the fracture zones. Within Fracture Zone 2, permeabilities range over six orders of magnitude, with high and low permeabilities appearing to form distinctive channels at the site scale (Figure 24). The prominent NE-trending transmissivity channel marks the intersection of this fault with Fracture Zone 2.5. The remaining channels are thought to result from some combination of structural controls and hydrogeological phenomena, such as the precipitation of infillings due to mixing of groundwaters with dissimilar chemistries. Areas of either high or low transmissivity appear as bands extending along the strike of the fracture zone.

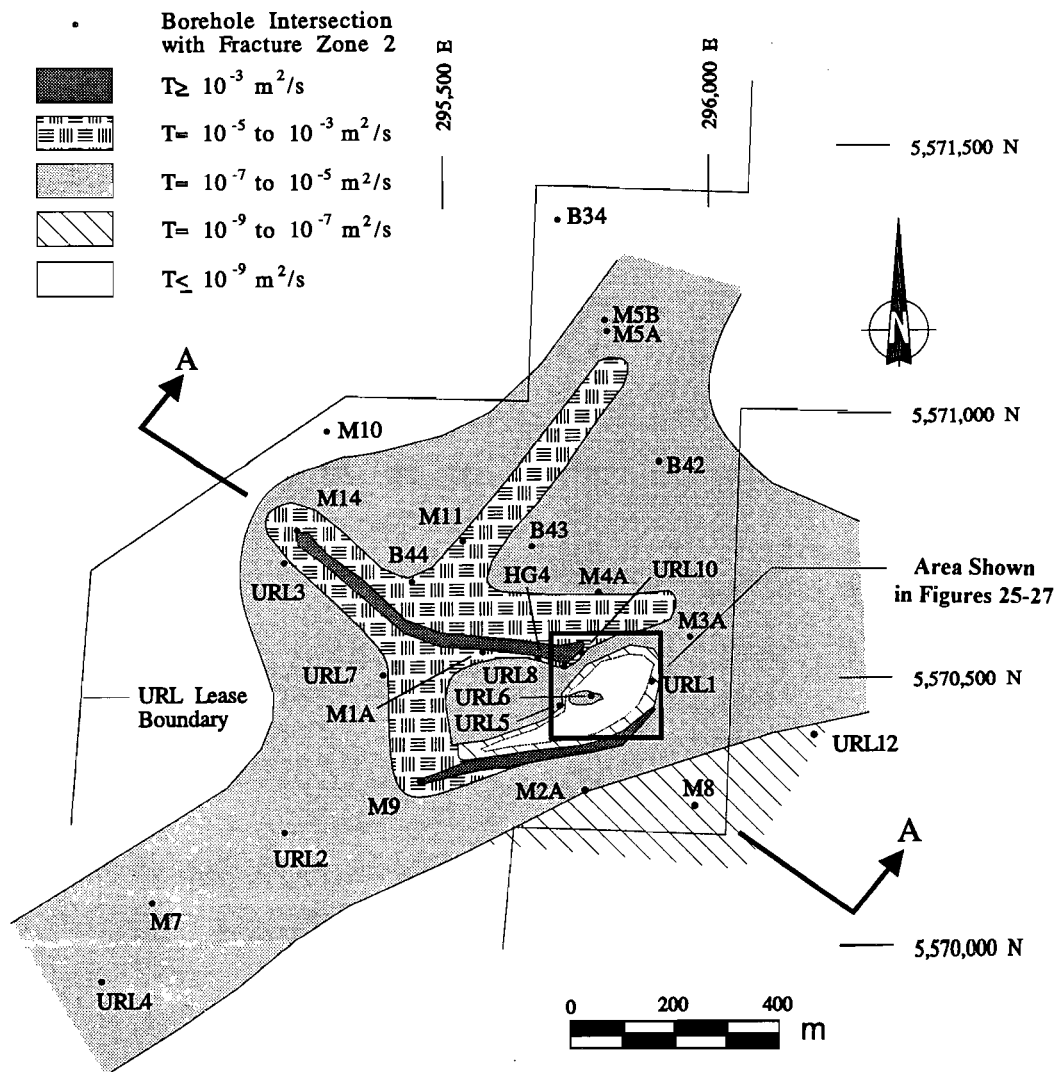


Figure 24. Variations in permeability within Fracture Zone 2.

The Solute Transport in Highly Fractured Rock Experiment defined a high transmissivity, low-storage zone that is located immediately northwest of the shaft (Figure 25). This zone is surrounded by extremely low transmissivity conditions, and it has very limited hydraulic communication with a much more extensive region of high transmissivity / high storage to the north and west.

These transmissivity anomalies are accompanied by:

- flexures in the fault zone, generalized here by structure contours representing the middle of the central cataclasite horizon,
- anomalies in the rock type hosting the fault (Figure 26); the fracture zone typically is confined to a xenolithic horizon (area 1 in Figure 26), but to the west and northwest the fracture zone changes in orientation such that it crosscuts the layering to intersect the neighbouring or gneissic granites, and
- occurrence of core discing in this area that represents locally high in situ rock stresses normal to the fault zone (Figure 27).

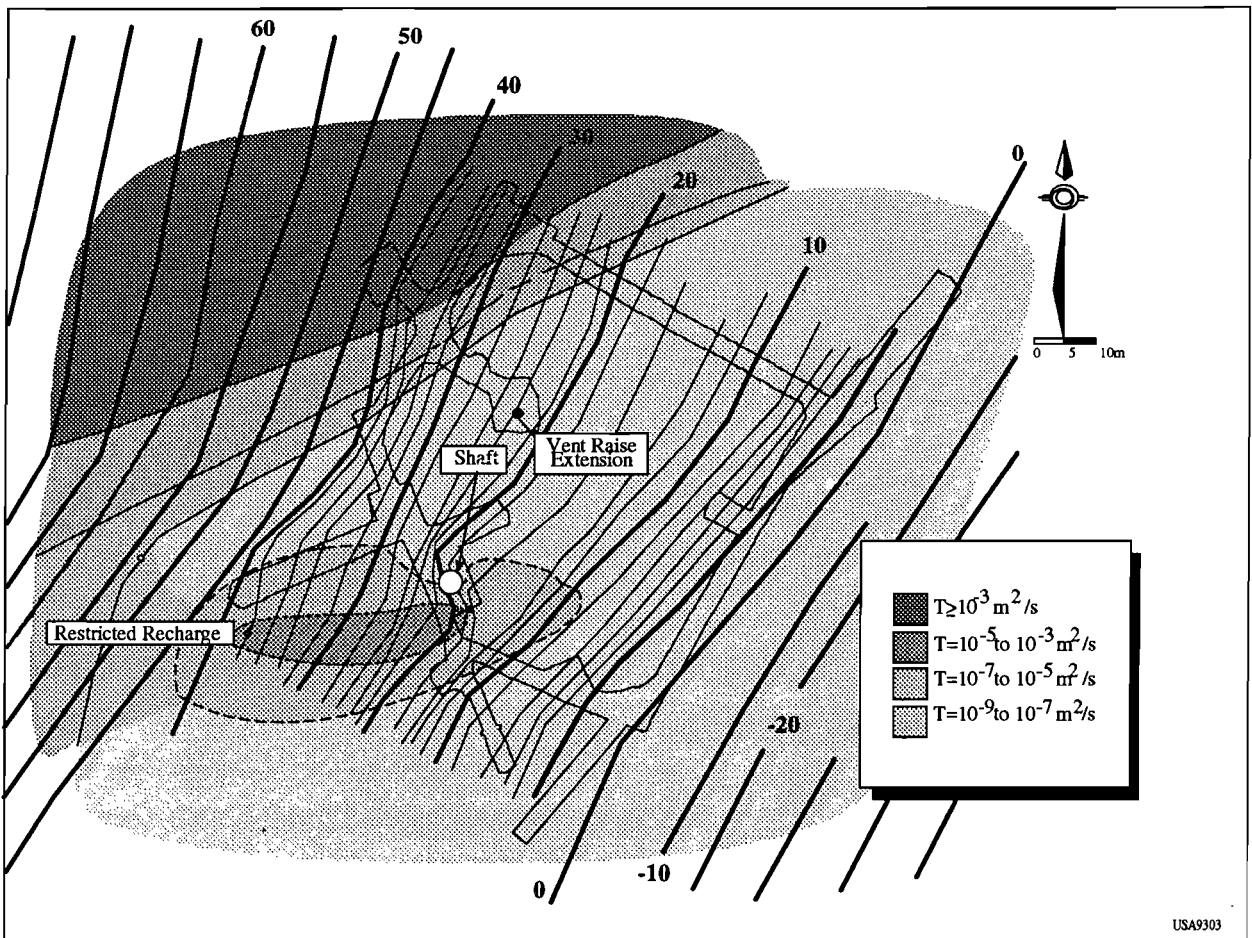


Figure 25. Variations in hydraulic conductivity within Fracture Zone 2 in the area below the 240 level. Contours show the elevation (m) for the top of Fracture Zone 2.

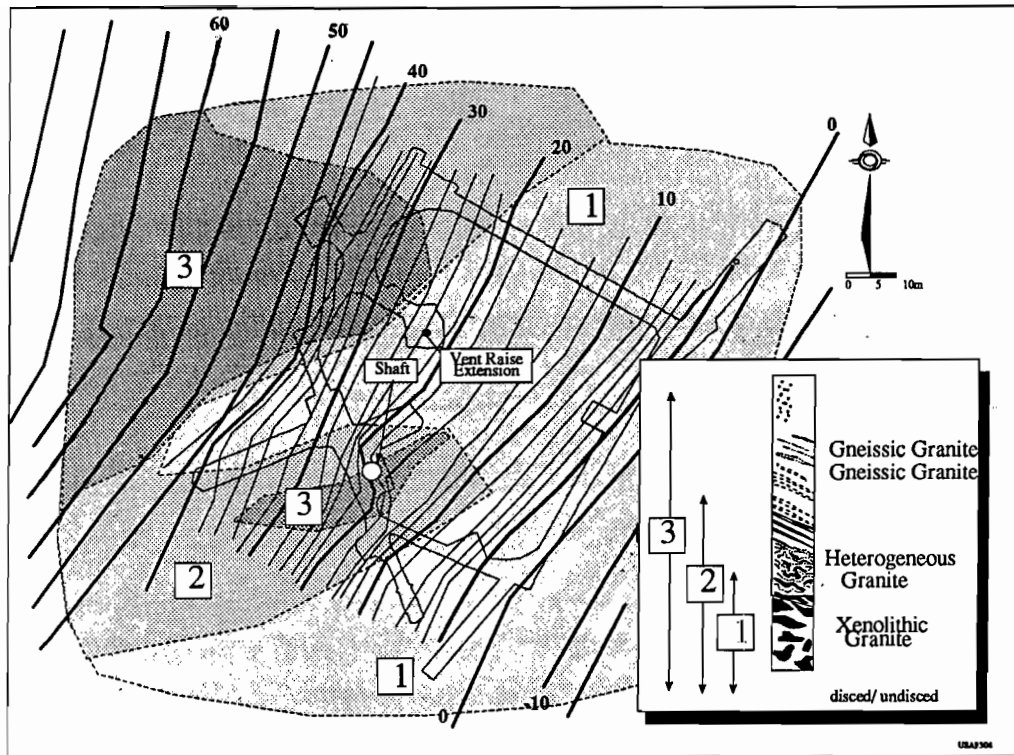


Figure 26. Map of the lithostructural domains hosting Fracture Zone 2 (Stop 12).

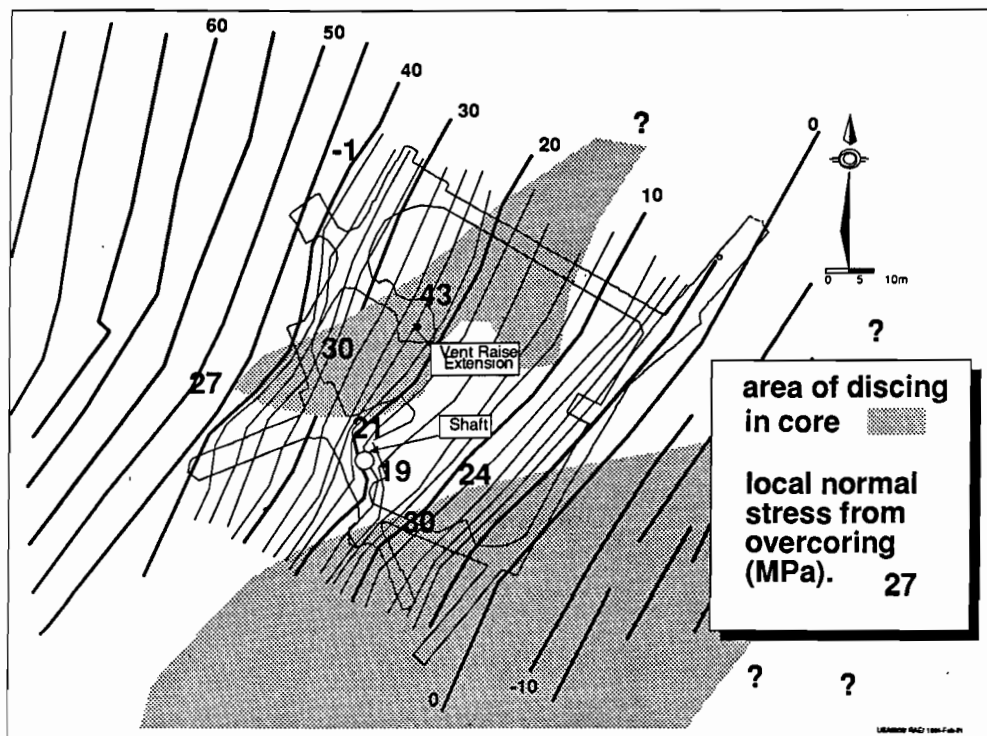


Figure 27. Areas of core discing and measured normal stresses (Stop 12).

It is concluded that the variations in the character and transmissivity of the fracture zones, and the variations in the stress magnitudes, are the direct result of undulations in the fault surface. As was shown in Figure 21, movement on any undulating surface can be expected to result in dilational gaps, restraining bends, fault-bounded structural wedges (such as that between Fracture Zone 2 and Fracture Zone 1.9), and secondary fractures in the fault-bounded blocks (such as the subvertical fracture in Room 219 in upcoming Stop 13).

Variations in relative transmissivity correspond to variations in the thickness of the alteration halo. This correlation is a useful one as it serves as a qualitative indicator of the historic flow variation, which has practical application in designing drilling programs and positioning excavations to minimize groundwater disturbance.

STOP 13: Special excavation techniques, prominent subvertical fracture in Room 209 (Quarried Block Fracture Migration Experiment)

This portion of the 240 Level was excavated for the Quarried Block Fracture Migration Experiment, which is sponsored by the Japanese Atomic Energy Research Institute (JAERI). The extremely smooth high-quality exposures at the end of the tunnel were produced by diamond wire cutting.

Features to note at this stop include:

- a prominent subvertical fracture (known as the Room 209 Fracture) at the transition from fractured to unfractured rock below Fracture Zone 2.5,
- the damage zone created directly ahead of a full face blast round, and
- lesser damage zone created adjacent to a pilot and slash round.

The Room 209 Fracture is significant in that it is the only water-bearing subvertical fracture between Fracture Zone 2 and Fracture Zone 2.5; the remainder of this block is effectively unfractured. The Room 209 Fracture comprises a wedge-shaped zone of fractures that begins at the base of Fracture Zone 2.5 and narrows downward until it terminates at the 240 Level, about 35 m above Fracture Zone 2. It parallels the strike of Fracture Zone 2, and extends 35 m vertically to the base of Fracture Zone 2.5, and at least 105 m horizontally. The fracture is thought to have formed in response to flexing of the fault block due to the change in dip angle of the fault directly beneath it. Such flexing would have led to a local reorientation of the principal stresses. The maximum principal stresses below and above the fault zone are perpendicular and parallel to the strike of the thrust fault, respectively. The stress field above the thrust fault is oriented so that the subvertical fractures in this zone are open and conductive.

The area in Room 219 cut by diamond wire saw provides a rare cross section of an excavation damage zone which in this case has propagated a distance of 3 m ahead of a tunnel face to intersect a subvertical water-bearing fracture 2 to 3 m from the excavation. Propagation of excavation damage bears directly on the design of excavations and the excavation method, as well as the integrity of the intact rock and any water-bearing fractures bordering the disposal area. The presence and time-dependent behaviour of any excavation damage also affect the design of excavation seals and other engineered barriers.

The geology and excavation damage visible in the walls as of 1995 June 05 are shown in (Figure 28). Blast-induced excavation damage consists of microcracks (hairline fractures) and whitened zones which stand out from the wall like miniature pop-ups. The relief of these pop-ups is very low -- less than 0.5 mm at most -- but they are clearly visible under low angle illumination. The whitening and relief appear to be grain- scale microcracking and dilation at the intersection of the cracks with the wall. This dilation appears to be time-dependent; the induced fractures had visibly advanced since photographs were taken in May 1995.

The extent of damage varies significantly between the northeast and southwest walls. This variation appears to be attributable to the type and orientation of the previous blast rounds. For example, the southwest wall (Figure 28a) provides a section along the centre-line and directly in front of a full face blast round. Remnants of the high energy production holes (bootlegs) are preserved on the tunnel face, and the cracks apparently propagate away from these points. Excavation damage, represented by hair-line cracking, has developed up to 3 m from the former tunnel face, and extends across the Room 209 Fracture. In contrast, the northeast wall (Figure 28b) is adjacent to a portion of tunnel excavated by slashing (controlled blasting along low energy perimeter holes). Excavation damage here is limited to a much less dense array of cracks confined to an area no more than 0.5 m from the tunnel wall.

On the southwest side of the tunnel, damage is concentrated in the upper two thirds of the wall. This may be a function of the location of blasthole remnants relative to the plane of section exposed, or to the timing of the blasts within this round. There may also be a structural control, as inspection of Figure 28a reveals that fractures normal to the Room 209 Fracture are preferentially developed, and that induced fractures in general are most frequent where the distance between the Room 209 Fracture and the blast round is at a minimum.

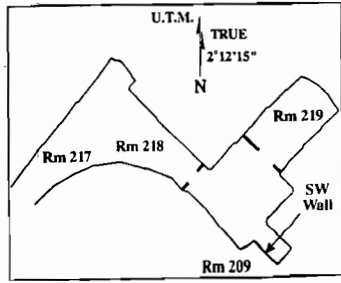
Local crack orientations are influenced by lithologic contacts and rock type, and this influence increases as the distance from the face increases. Although coarse feldspars are particularly prone to microcracking, there is no other clear tendency for one rock type to be more fractured than another.

STOP 14 (Optional): Fracture Zone 2 in the shaft, 270m depth.

This stop is in the access shaft between 270 and 290m, at its intersection with Fracture Zone 2 (Figure 29). Fracture Zone 1.9 (Figure 7), slightly below this point, is a minor splay within the footwall of Fracture Zone 2 (Figure 21). *Access to these locations is limited under normal circumstances, and will be at the discretion of Site Operations.*

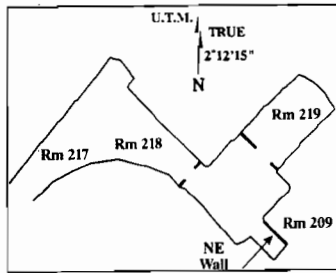
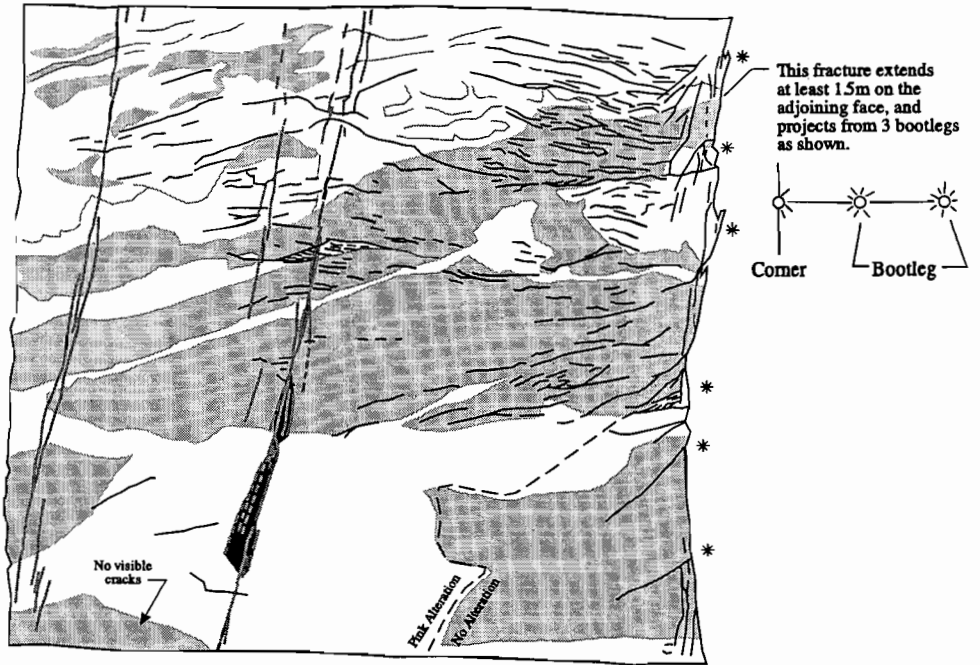
The general structure and total offset of Fracture Zone 2 are shown in Figure 30, a cross section normal to its strike. Bracketed numbers (e.g.:{3}) refer to the annotations in the figure. Features depicted include:

- {1} cataclasite and weathered rubble zone,
- {2} limits of subvertical and low-dipping fractures in hangingwall and footwall,
- {3} alteration halo in the unfractured rock surrounding the fault,
- {4} unfractured and unaltered granite.



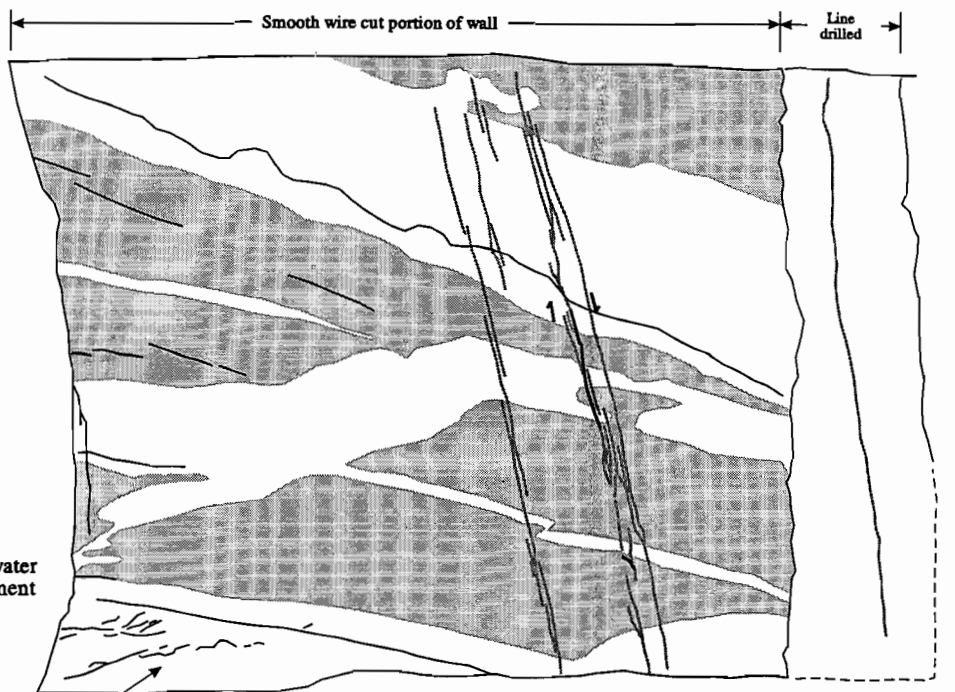
Location Map

A



Location Map

B



Legend

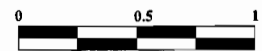
Natural Fractures, open water bearing segment

Induced Fractures

Rock Unit Boundary

Heterogeneous Pegmatite

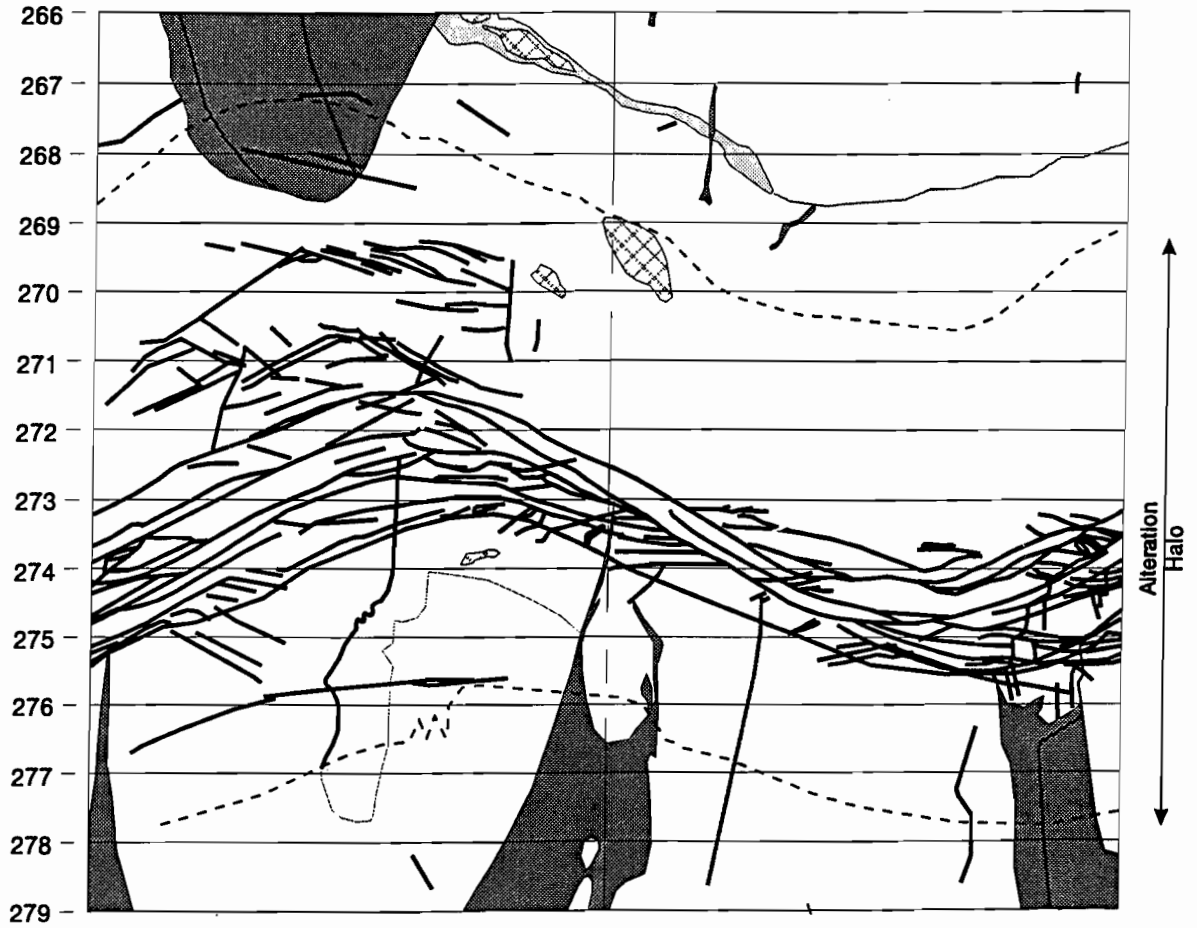
Homogeneous Granites of various types



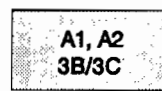
Scale in metres

Figure 28. Geology and excavation damage in a tunnel segment cut by diamond wire saw at the 240 level (Stop 13): (A) southwest wall adjacent to full-face blast round, (B) northeast wall adjacent to pilot-and-slash-round.

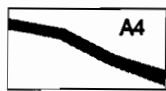
Depth from Shaft Collar



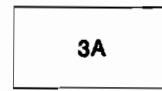
Fractures



A1, A2
3B/3C
Leucocratic
Granite dykes
or sills



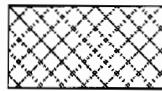
A4
Pegmatite
Dykes



3A
Gneissic Granite



7A
Granodiorite
Dykes



Amphibolitic
Xenoliths

Figure 29. Simplified geological map of Fracture Zone 2 as seen in the URL access shaft (Stop 14).

A granodiorite dyke {5}, intersected by the shaft and by several boreholes, is displaced 7.3 m by reverse dip-slip movement along the fault. The extent and relative orientation of subsidiary, hematite-filled fractures are also shown {6,7}. The direction of slip is indicated by the 90° pitch of slickenlines and other lineations on the fault surface, by dilational gaps, and by numerous intersections of the displaced dyke and fault zone by cored boreholes (only boreholes GC-5, GC-7 and GC-8 are shown). It is also confirmed by the incremental movement visible within the fault (enlarged section of Figure 30). Also shown in this enlargement are {8} - the cataclasite material, {9} - the major chloritic slip surfaces, and {10} - the subsidiary, hematitic fractures.

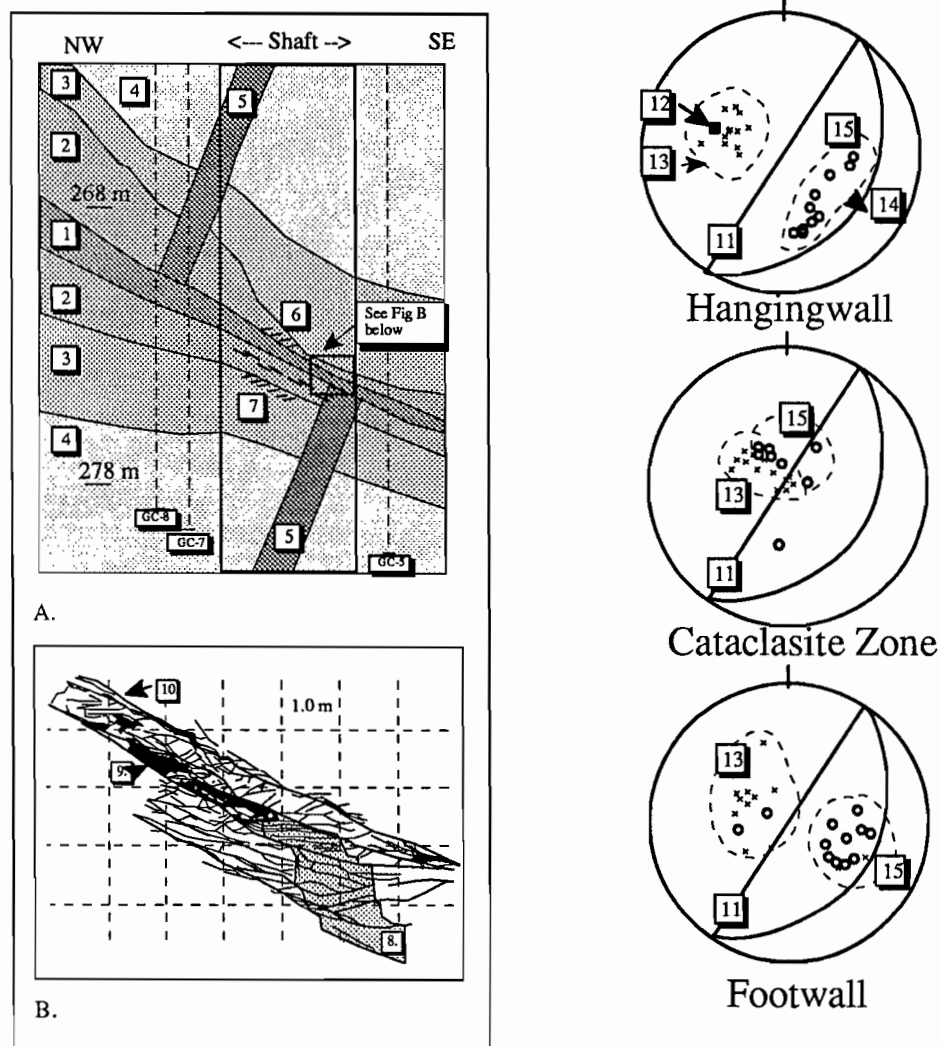


Figure 30. General structure and total offset of Fracture Zone 2 as seen in a cross section normal to its strike (Stop 14). Explanation of numbers on stereonets: 11 - average plane of FZ2; 12 - pole to average plane of FZ2; 13 - poles to chloritic slip surfaces within fault; 14 - lineations on 13; 15 - open circles - poles to hematitic fractures. Other numbers, in boxes, are described in the text.

Most chloritic fractures and slip surfaces parallel the large-scale fault orientation and the compositional layering in the granite. Subsidiary fractures in the footwall and hangingwall are predominantly hematite-filled, show no offset, and terminate within 1 to 2 m of the fault. They either parallel the fault zone, dip toward it with a dihedral angle of 20°-30°, or are low-dipping.

STOP 15: Granodiorite dykes in grey granite, excavation damage fractures at the 300 Level

The 300 Level Shaft Station (Figure 4) is located in unfractured grey granite below Fracture Zone 2. The grey granite here is cut by three generations of auto-intrusive dykes, the most noteworthy of which, a granodiorite swarm, is the predominant lithology at this stop. The host phase of the batholith is represented by angular inclusions of granite and by variously disrupted blocks between the dykes.

Special efforts were made during the excavation of the 300 Level Shaft Station to optimize the amount and quality of exposure available in order to characterize the damage zone around the circular access shaft. Prior to construction of the 300 Level Shaft Station, the shaft was excavated to a depth of about 15 m, or 3 shaft diameters below the floor of the station to accommodate any time-dependent behaviour in the formation and propagation of the excavation damage, and to avoid the effect of stress concentration. The 300 Level Shaft Station access station was then excavated using controlled pilot and slash techniques for the walls, floor, and crown. This was done to duplicate the quality of excavation characteristic of the shaft, and to avoid inadvertent excavation of damaged rock. Two surfaces were then made available for observation of the excavation damage zone about the shaft perimeter. These were a temporary 90° brow formed by the intersection of the shaft walls and the station crown (once photographed, this was trimmed to a more stable 45° slope), and the station floor. A third area, referred to as the station lip and lip pocket, provided a sample of the damage zone beneath the floor of the station as seen from the shaft walls. The results of the excavation damage zone mapping are shown in Figure 31. Although it may be possible to distinguish in outcrop certain specific fractures that originated either through excavation-induced stress or through blasting (chiefly on the basis of location and pattern), most fractures are likely to be the result of a combination of processes.

The excavation damage zone about the circular shaft extension was mapped during the excavation of this station. The reduction in damage zone thickness compared to that seen in the previous rectangular shaft is attributed to improvements in excavation methods, to conversion to a circular cross section, and to increasing isotropy of stresses with depth. Damage distribution may be correlated with rock fabric and with the principal stress orientations.

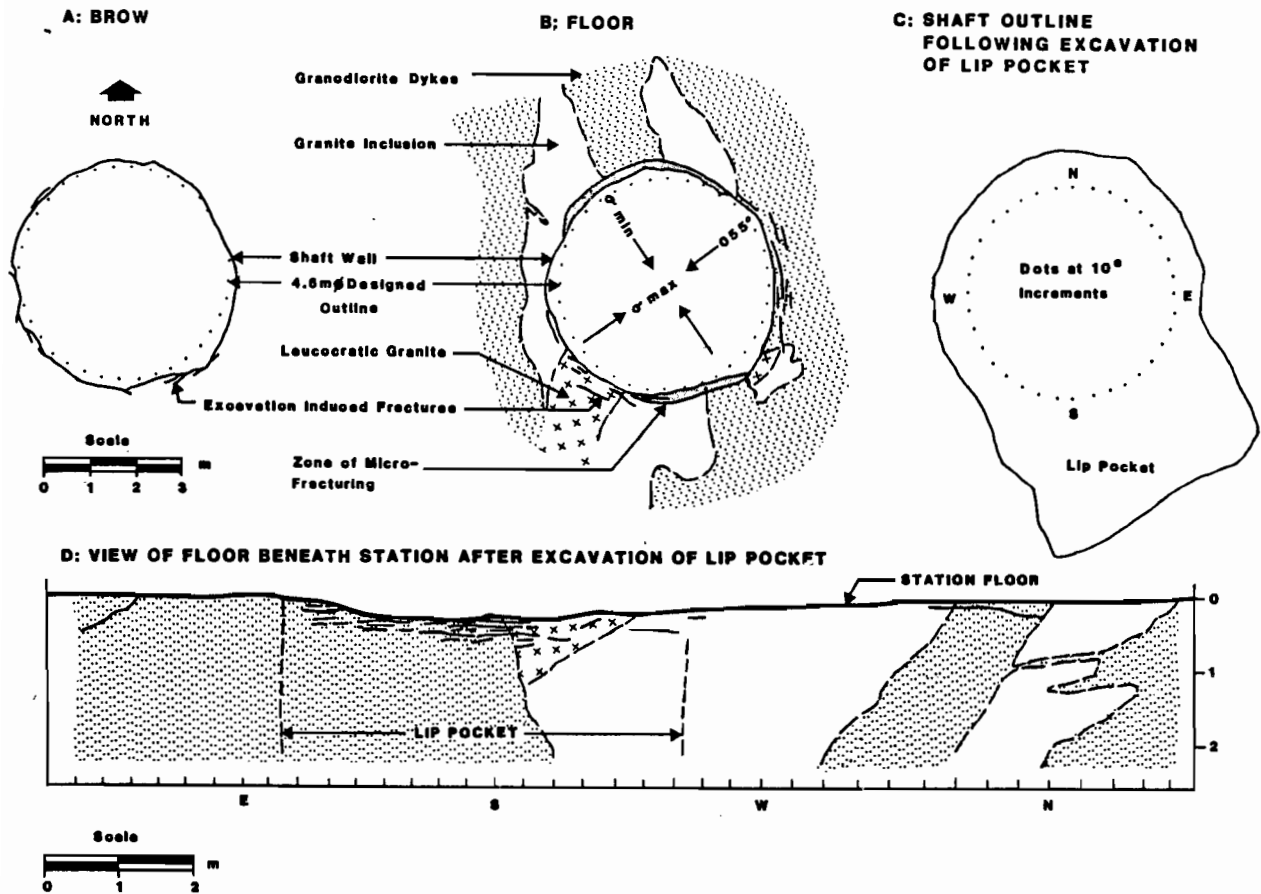


Figure 31. Simplified geological map showing the excavation damage at the 300 Level station (Stop 15).

STOP 16: 420 Level Station: Geology of the 420 Level.

General Geology

Rock units present at the 420 Level (Figure 4) include gneissic, leucocratic and minor xenolithic granite. These are crosscut by granodiorite dykes, which are in turn host to pegmatite dykes and quartz veins. Large-scale layering persists at this depth in the batholith, but xenolithic and heterogeneous zones are less common than at higher levels. Exploration drilling from the 420 Level to depths greater than 1000 m indicates that this trend continues at depth.

Five major litho-structural domains, classified as domains 14 through 18, are recognized at the 420 Level (Figure 32):

- Domain 14 **Gneissic grey granite.** This domain is medium grained, weakly gneissic to massive, with up to 10% biotite and magnetite. The out-crop-scale layering or gneissosity has an average orientation of 172°/19°.
- Domain 15 **Xenolithic-leucocratic granite.** The predominant rock type in this domain is a schlieric to variously gneissic, grey, leucocratic granite. Biotite and magnetite make up less than 2% of the mineralogy. The texture ranges from medium-grained to pegmatitic. Metavolcanic xenoliths are flattened in the plane of the compositional layering, which is oriented between 195°/25° and 076°/14°. The upper contact of this domain crosscuts the layering in Domain 14, is oriented 178° / 33°, and is marked by a porphyroblastic zone up to 350 mm thick. The porphyroblasts (feldspars) range up to 80 mm in size, and are weakly saussuritized. The lower contact is also discordant, and has an average orientation of 110°/34°.
- Domain 16 **Gneissic grey granite.** This domain is similar to domain 14. The granite fabric ranges from weakly gneissic to locally massive. The orientation of the gneissosity varies between 110°/27° and 101°/36°. The contacts between this domain and the surrounding leucocratic granites are largely obscured by granodiorite dykes that follow the layering.
- Domain 17 **Leucocratic granite.** This domain is similar to leucocratic granite domain 15, but is not xenolithic. The fabric in this domain ranges from weakly gneissic to locally massive, with the gneissosity averaging 128°/21°. The upper contact of this domain, oriented 203°/20°, is sharp and apparently concordant with the structure in Domain 16. The lower contact of this domain is a transition zone, marked by 1.2 m of interlayered leucocratic and gneissic granite, with these layers oriented 108°/27°.
- Domain 18 **Gneissic grey granite.** This domain is similar to domains 14 and 16. Gneissosity is weakly developed, and averages 177°/27° and 101°/36°. The contacts between this domain and the surrounding leucocratic granites are largely obscured by granodiorite dykes that follow the layering.

The granodiorite dyke swarm crosscuts these litho-structural domains and is widespread throughout the 420 Level. One dyke exposed in Room 406 has a width of approximately 15 m. The gneissic granite adjacent to the dyke has been fragmented and disrupted, with granite fragments separated by a network of granodiorite seams.

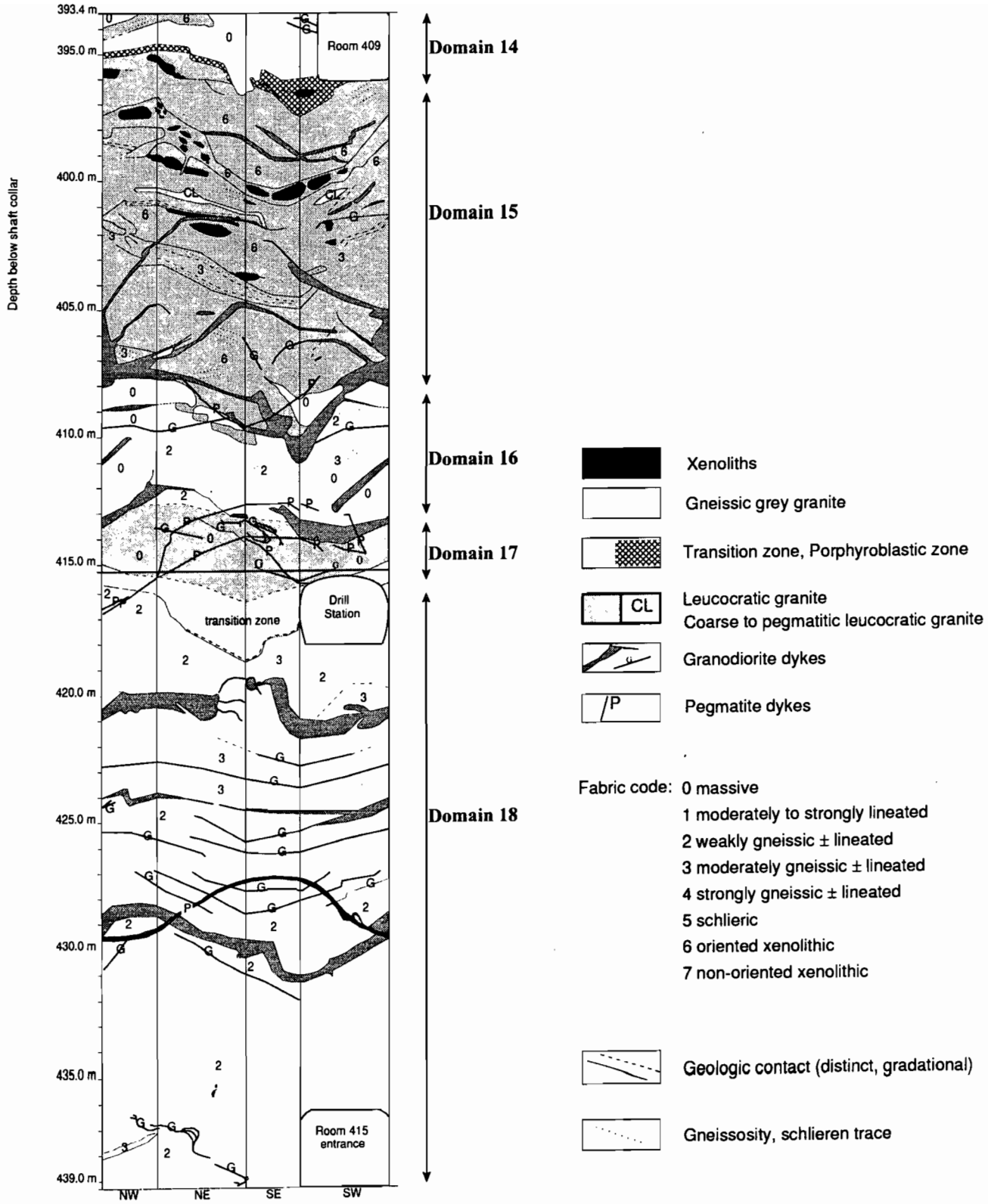


Figure 32. Simplified geological map of the 420 Level Crib Raise showing litho-structural domains (Stop 16).

This disrupted zone is 8 m wide in Room 406, and approximately 3 m wide elsewhere on this level. The granodiorite dykes have two average orientations: 178°/70° W and 158°/26° SW. The latter orientation is seen only at the 420 Level.

Pegmatite dykes crosscut all other rock types but are mostly confined to the larger granodiorite dykes at this level. They are quartzo-feldspathic with euhedral to subhedral biotite and magnetite that may constitute up to 10% of the mineralogy. Sphene is also present in trace amounts. The pegmatites are usually planar and thin (orientation of 018°/74° NW). Some normal offset is associated with the pegmatites but offset magnitudes do not exceed several millimetres.

Fractures

The locations of Fracture Zones 1 and 1.5 relative to the 420 Level are not known precisely, due to the limited number of borehole intersections with each structure. Borehole intersections with Fracture Zone 1 are 500 m up-dip from the shaft. The fracture zone is thought to terminate down-dip and/or along strike and so does not intersect the 420 Level or any of the exploration boreholes drilled from the excavations. Fracture Zone 1.5 was intersected in several boreholes located 124 to 192 m from the 420 Level. The fracture zones consist of several low-dipping, chloritic and hematitic fractures. The adjacent rock displays the characteristic groundwater-induced reddish alteration halo typical of other major water-bearing zones, but there is almost no seepage from this zone. The extent of this zone beyond these intersections is poorly defined. Low-dipping, apparently coplanar fracture zones have been intersected to the north, south and west of the excavations, but not in the shaft or in neighbouring boreholes. It is possible that the intersections identified represent subparallel but distinctly separate surfaces.

Only six natural fractures have been encountered within or between the 420 Level excavations. All are confined to the granodiorite dyke swarm, where they are thought to be cooling fractures formed by parting along compositional layering within the granodiorite dykes. The six fractures are dry and tight, and were apparently closed until opened by either drilling or excavation. Infillings include sericite, chlorite, and carbonate. Sulphides exposed on the fracture surface are unoxidized. A low-plunging mineral lineation was observed on the fracture surface at each intersection.

Excavation damage

Excavation damage is found to varying degrees at all levels of the URL, but stress-induced spalling is particularly well displayed at the 420 Level with notches or breakouts in the crowns of various rooms. Notch margins are defined by relatively planar induced fractures, between which progressive spalling of thin tabular slabs has occurred. Within the V-shaped apex of each notch, the granite has been "crushed" to thin slivers, which are oriented approximately parallel to the margins of the "V". The location and pattern of notch development appear to have resulted primarily from the in situ stress magnitudes and orientations in combination with a number of factors, including the sequence of excavation, room geometry, and variations in local geology. The notch that developed just south of the shaft, for example, appears to align with the margin of a granodiorite dyke. Variations in notch development may also be attributable

to the slightly higher uniaxial compressive strength of the granodiorite (225 ± 20 MPa) relative to the other rock types (213 ± 20 MPa) (Read and Martin 1992). The distribution of rock types and the degree and orientation of foliations are considered in experiment and excavation design.

STOP 17: Excavation damage study, Room 405

A 1.2m diameter borehole was drilled 5 m into the floor of a typical drill-and-blast tunnel in unfractured granite. This borehole provides a cross-section through the blast-and stress-induced damage zone beneath the floor of the tunnel, as well as examples of borehole damage formed during and after drilling (Figure 33). The tunnel is a conventional drill-and-blast tunnel with a horseshoe-shaped cross section. The tunnel was widened from 3.4 to 5.0m by slashing the northwest wall. The borehole straddles the lower right corner of the original tunnel profile. Two core segments totaling approximately 1.3m of disced, weakly gneissic grey granite were retrieved. The balance of the core was disced to the extent that it disintegrated into rubble and had to be removed from the borehole manually.

Three generations of excavation damage, each with their own distribution and geometry, are present.

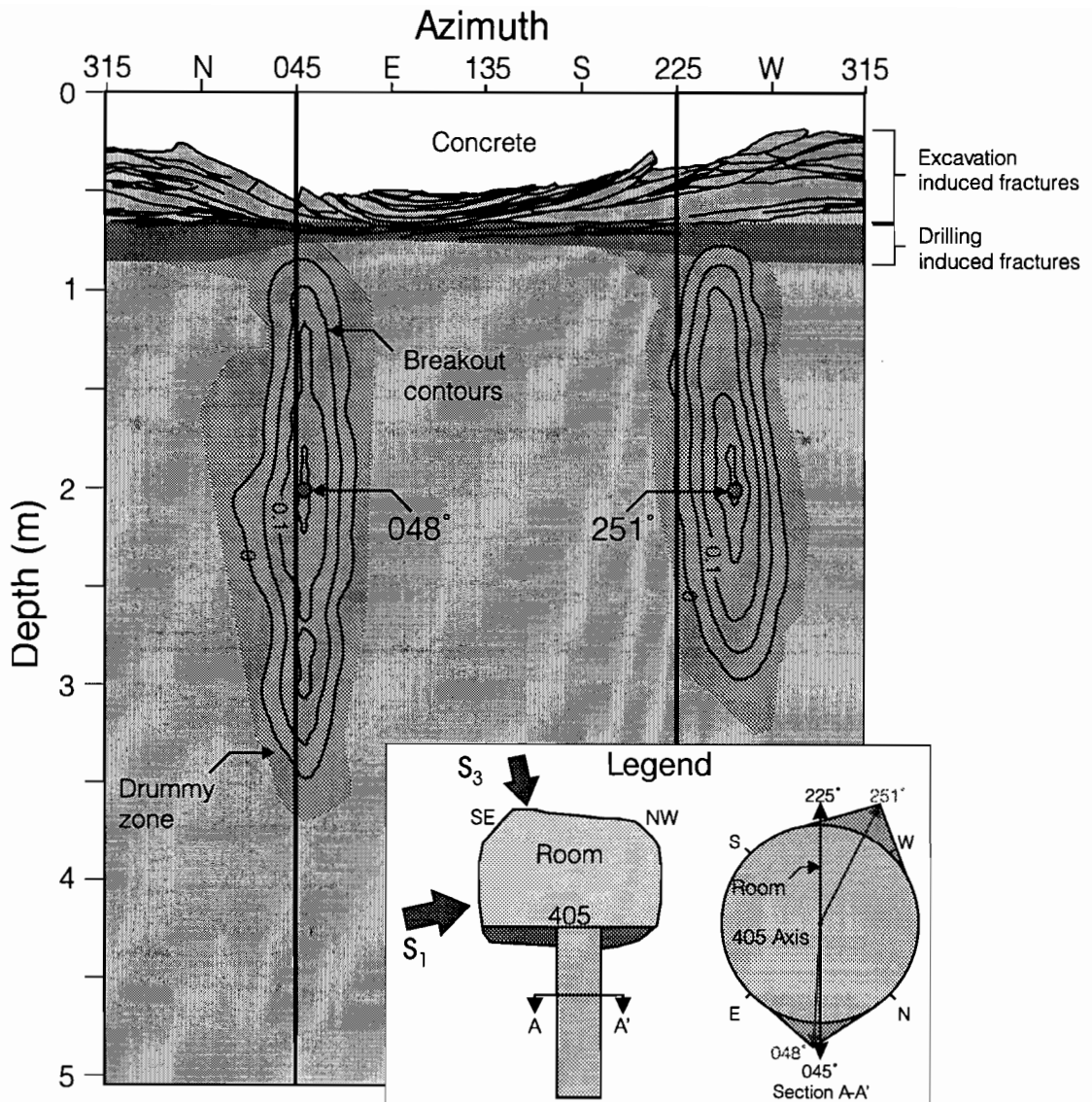
Tunnel Excavation Damage

The excavation-damage zone formed during the initial excavation and subsequent widening of the tunnel is confined to the top 300 to 400 mm of the borehole below the concrete. Within this zone there are from 11 to 17 induced fractures, some of which are partially filled with concrete that had seeped down during the pouring of the floor. These fractures are generally low-dipping but their dip decreases with depth such that, at the base of the damage zone, most fractures have curved into parallelism with each other and with the average excavation surface. This observation is significant for estimating damage zone thickness, and for modelling and interpreting its hydraulic conductivity.

Displacement across the SE-dipping induced fractures is indicated by small (<2mm) dilational gaps. The displacement, although very small, (<0.5mm), is sufficient to indicate that the direction of movement is reverse-dip-slip, with the overlying blocks moving to the northwest relative to the underlying blocks. In relative terms, this means the floor slabs moved toward the floor notch. It is not possible to determine if this movement took place in one or more, episodes, or if it is directly related to tunnel floor notch development, but the displacement is consistent with the measured stress magnitudes and directions. It is also consistent with observations in Room 415 (Stop 18).

Borehole Drilling-Related Damage

Horizontal, closely spaced (<10mm) fractures were encountered in both the core and the 100- to 150-mm section of the borehole wall directly below the tunnel floor excavation damage zone (Figure 33). These fractures differ from the tunnel-related induced fractures above them in several respects; (1) the planarity of their surfaces, (2) the absence of fracture splay development, (3) their extremely tight spacing, (4) the absence of detectable offset, and (5) their high degree of parallelism with each other.



1.24-m diameter Borehole in Room 405

Asymmetry

- breakouts develop near advancing face during drilling
- at 2-m depth, azimuths of NE and SW breakouts 048° and 251°, respectively
- NE and SW breakouts extend to depths of 3.50 and 2.96 m, respectively
- angular asymmetry of 23° at 2-m depth
- asymmetry in breakout lengths 0.54 m

Figure 33. Perimeter map showing excavation damage breakout contours and general fracture orientation in the Room 405 borehole (Stop 17). The inset shows the location of the borehole relative to the tunnel profile.

Given the dissimilarity between these fractures and known stress-induced (extensional) floor fracturing, it is concluded they were probably initiated during drilling. The process would have involved simultaneous initiation of fractures from the high stress concentrations developed at the thin-walled drillbit tip into both the borehole wall and the core (where it would be responsible for core discing). Having thus developed, these borehole wall fractures may have subsequently been propagated by extensional fracturing attendant with floor uplift.

Borehole Breakout Notches

Two breakout zones have developed in the borehole at azimuth 048° and 251° approximately parallel to the tunnel axis, and nearly perpendicular to the maximum horizontal stress at this level (Read et al. 1995). These breakouts begin within or just below the discing zone, and have propagated to a maximum depth of 3.5 m (Figure 33). The breakouts are a result of stress concentrations around the tunnel being magnified by additional stress concentrations around the borehole. Notch formation occurs during drilling, and ceases at the point where the tangential stress at the notch tip, resulting from the combined influence of the room and borehole, equals the in situ rock strength.

Active propagation of the notches occurs within and at the lower end of each notch apex primarily during drilling, by grain-scale microcracking and dilation of the granite. At the lower end of the notches, this "failure initiation zone" bulges up to 15 mm into the borehole cavity. Seepage from the damage zone beneath the concrete-granite contact collects in this area, and possibly contributes to breakout advance.

The breakouts in this and other vertical holes are asymmetric, i.e., not diametrically opposed. This observation is consistent with other findings at the URL which suggest that the deviatoric stress ahead of the advancing borehole face contributes to the development of damage around the borehole. This damage influences the development of borehole breakouts and, for holes not aligned with a principal stress direction, reflects the asymmetric pattern of stresses ahead of the borehole during drilling.

STOP 18: Mine-by Experiment, Room 415

The Mine-by Experiment is being conducted, in part, to investigate the characteristics of the excavation damage zone that forms during construction of underground openings in crystalline rock (Read and Martin 1996). The experiment, which has been in progress since 1989, has had three phases - the excavation response study, the connected permeability study and the heated failure study.

The excavation response study is one of the foremost rock mechanics experiments in the world, and the first to control temperature, excavation geometry and excavation method to facilitate interpretation of the experimental results. It was conducted at the 420 Level of the URL to investigate the response induced in the rock mass by excavating a 3.5-m-diameter circular tunnel using a non-explosive technique. The main objective of the experiment was to study the processes involved in progressive failure and the development of excavation-induced damage around underground openings. To this end, state-of-the-art geomechanical and geophysical instrumentation was used to monitor the excavation of the 46-m-long Mine-by Experiment test tunnel.

An essential feature of this type of experiment is that instrumentation is installed and operating prior to excavation of the tunnel. In this way, it is possible to monitor the complete excavation-induced response of the rock mass, including effects ahead of the advancing tunnel face.

The results from the experiment show that progressive failure in compressive regions around the tunnel initiates at stresses about 50% of the rock strength measured in uniaxial compression tests in the laboratory. The difference between the laboratory and in situ behaviour is attributed to complex stress changes that occur during excavation of the tunnel, especially in the vicinity of the advancing face. These effects are not simulated in standard laboratory tests. Numerical modelling and in situ characterization studies were conducted to establish the extent and characteristics of the damaged zone around the test tunnel. As part of this study, in situ stresses and material properties were established through back analysis of measured displacements and strains. Using these boundary conditions, it was shown that the damaged zone was limited to within 1 m of the original tunnel perimeter. The characteristics of the damaged zone, however, were found to be highly variable around the tunnel, and were dependent on the nature of the stress concentrations, geology, stress magnitudes and orientations and, to a lesser extent, the excavation method and sequence. Beyond the damaged zone, the rock mass behaves in a linear elastic manner with strength properties comparable to those found in the laboratory.

The following types of excavation damage have been observed in the Room 415 tunnel to date:

- breakout notches in the crown and floor of the tunnel,
- a stress-induced sub-horizontal fracture which propagated from the pilot borehole, along the plane of gneissosity, prior to excavation,
- similar stress-induced fractures in Face 0 of Room 415,
- stress-induced damage to the line-drilling boreholes, and
- excavation-induced fractures of uncertain origin (i.e. blasting and/ or stress redistribution) on the tunnel surface.

The connected permeability study is designed to characterize the flow properties of the excavation-induced damage zone in granitic rock. As part of this study, a 1.5 m high concrete dam was formed on the floor of the Mine-by test tunnel, and the gallery behind the dam was filled with water. The water was allowed to flow underneath the concrete dam and through the damaged zone under the floor of the excavation, after which it was collected in troughs on the downstream side. The hydraulic properties of the excavation damaged zone were characterized by comparing the quantity of water that moved through the damaged rock during tests involving different flow path lengths created by widening the dam in stages. The testing has indicated that all of the flow in this experiment occurred very near the surface of the excavation, either through surface-parallel fractures or through a small zone of highly fractured rock at the surface. Although the damage zone is hydraulically connected throughout its length, virtually no flow takes place in the rock at depths greater than 15 cm below the floor.

The heated failure study was designed to investigate the effects of thermally-induced stresses on progressive failure in large-diameter vertical boreholes excavated in highly stressed rock. Preliminary results from acoustic emission (AE) monitoring

indicate that progressive failure in the rock is affected by the stress path near the borehole face during drilling. Boreholes that were heated prior to drilling experienced more extensive breakouts than boreholes that were heated after drilling. The study also found that the combination of stresses from two adjacent boreholes can increase the extent of progressive failure, both radially and vertically, in the web of rock separating the two holes. Breakouts in this case extended to a maximum radial distance of 10 cm, resulting in a decrease of 40% in web thickness. Breakouts also extended the full 4-m depth of the boreholes in this case.

The Room 415 tunnel geology is depicted in Figure 34. The tunnel is excavated in unfractured and unaltered gneissic grey and leucocratic granite. Orientation of the gneissic layering is highly variable due to disruption by the granodiorite dykes. The contact zone (about 9.7 m thick) between the leucocratic and gneissic granites, is oriented 034°/23° SE. The granodiorite and pegmatite dykes have average orientations of 052°/85° NW and 028°/66° NW, respectively.

The granodiorite dyke swarm has disrupted the layering of the earlier granites to a considerable degree. As much as 4 m of reverse dip-slip separation of the gneissic granite/ leucocratic granite contact is visible at the entrance of the Mine-by tunnel. Within Room 415, the grey and leucocratic granites occur as either variably oriented fragments in a granodiorite groundmass, or as disrupted blocks in a network of granodiorite dykes.

Only one natural fracture has been encountered in the test tunnel. It covered the lower half of face 24, but it is no longer visible because it did not extend to either the walls or crown. This fracture contained a chlorite-sericite infilling, and was oriented 130°/84° NE, approximately coincident with the flow banding in the dyke.

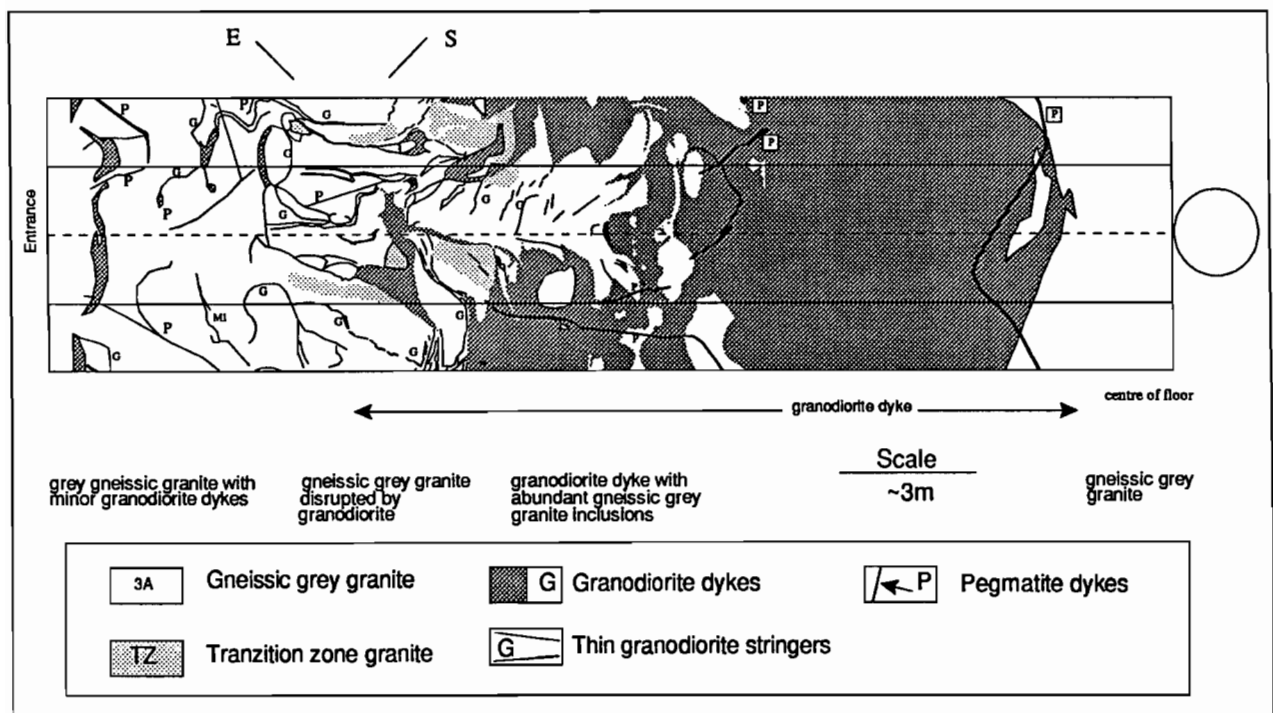


Figure 34. Geological map of the Mine-by Experiment test tunnel (Stop 18).

ACKNOWLEDGMENTS

We would like to thank Denver Stone, Jan Cramer, Mel Gascoyne, Paul Thompson, and Rod Read for their constructive comments and advice in preparing this guidebook. We also thank G.Hiltz and E.Jacobs for their assistance in providing the figures. The work was funded jointly by AECL and Ontario Hydro under the auspices of the CANDU Owners Group (COG).

REFERENCES

- AECL (Atomic Energy of Canada Limited). 1994. Environmental impact statement on the concept for disposal of Canada's nuclear fuel waste. Atomic Energy of Canada Limited Report AECL-10711, COG-93-1.
- Ayres, L.D. 1978. Metamorphism in the Superior Province of northwestern Ontario and its relationship to crustal development. *In* Metamorphism in the Canadian Shield. *Edited by* J.A. Fraser and W.W. Heywood. Geological Survey of Canada, Paper 78-10, pp. 25-36.
- Beakhouse, G.P. 1977. A subdivision of the western English River Subprovince. *Canadian Journal of Earth Sciences* **14**: 1481-1489.
- Beakhouse, G.P. 1985. The relationship of supracrustal sequences to a basement complex in the western English River Subprovince. *In* Evolution of Archean supracrustal sequences. *Edited by* L.D. Ayres, P.C. Thurston, K.D. Card, and W. Weber. Geological Association of Canada Special Paper 28, pp. 169-178.
- Beakhouse, G.P., McNutt, R.H., and Krogh, T.E. 1988. Comparative Rb-Sr and U-Pb zircon geochronology of late- to post-tectonic plutons in the Winnipeg River Belt, northwestern Ontario, Canada. *Chemical Geology*, **72**: 337-351.
- Brisbin, W.C. 1979. A gravity profile across the Lac du Bonnet Batholith in southeastern Manitoba. Atomic Energy of Canada Limited, Technical Record TR-17.*
- Brown, A., and Soonawala, N.M. 1982. Geology of the Underground Research Laboratory Site, Lac du Bonnet Batholith, southeastern Manitoba. Geological Association of Canada - Mineralogical Association of Canada Field Trip Guidebook 15, 20 p.
- Brown, A., Everitt, R.A., Martin, C.D., and Davison, C.C. 1995. Past and future fracturing in AECL research areas in the Superior Province of the Canadian Precambrian Shield, with emphasis on the Lac du Bonnet Batholith. Atomic Energy of Canada Limited Report, AECL-11214, COG-94-528.*

- Brown, A., Soonawala, N.M., Everitt, R.A., and Kamineni, D.C. 1989. Geology and geophysics of the Underground Research Laboratory site, Lac du Bonnet Batholith, Manitoba. *Canadian Journal of Earth Sciences* **26**: 404-425.
- Card, K.D., and Ciesielski, A. 1986. DNAG #1. Subdivisions of the Superior Province of the Canadian Shield. *Geoscience Canada* **13**: 5-13.
- Cerny, P., Fryer, B.J., Longstaffe, F.J., and Tammemagi, H.Y. 1987. The Archean Lac du Bonnet Batholith, Manitoba: Igneous history, metamorphic effects, and fluid overprinting. *Geochimica et Cosmochimica Acta*, **51**: 421-438.
- Cerny, P., Trueman, D.L., Ziehlke, D.V., Goad, B.E., and Paul, B.J. 1981. The Cat Lake-Winnipeg River and Wekusko Lake pegmatite fields, Manitoba. Manitoba Department of Energy and Mines, Mineral Resources Division, Economic Geology Report ER80-1.
- Corfu, F., and Andrews, A.J. 1988. Differential response of U-Pb systems in minerals, Winnipeg River Subprovince, Canadian Shield: implications for Archean crustal growth and stabilization. *Contributions to Mineralogy and Petrology*, **98**: 312-325.
- Davis, D.W., Corfu, F., and Krogh, T.E. 1986. High precision U-Pb geochronology and implications for the tectonic evolution of the Superior Province. In *Workshop on tectonic evolution of greenstone belts*. Edited by M.J. deWit and L.D. Ashwal. Lunar and Planetary Institute, Houston, TX, Technical Report 86-10, pp. 77-79.
- Davis, G.H. 1984. *Structural geology of rocks and regions*. New York: John Wiley & Sons.
- Davison, C.C. 1982. Hydrogeological studies at the URL site. In *The Geoscience Program - Proceedings of the Twelfth Information Meeting of the Nuclear Fuel Waste Program*. Atomic Energy of Canada Limited Technical Record, TR-200*, Volume II, pp. 332-353.
- Davison, C.C., Chan, T., Brown, A., Gascoyne, M., Kamineni, D.C., Lodha, G.S., Melnyk, T.W., Nakka, B.W., O'Connor, P.A., Ophori, D.U., Scheier, N.W., Soonawala, N.M., Stanchell, F.W., Stevenson, D.R., Thorne, G.A., Whitaker, S.H., Vandergraaf, T.T., and Vilks, P. (1994). The disposal of Canada's nuclear fuel waste: The geosphere model for postclosure assessment. Atomic Energy of Canada Limited Report AECL-10719, COG-93-9.*
- Everitt, R.A., Chapman, A.E., Northrop, P., and Brown, A. 1987. Geology of the Underground Research Laboratory ventilation raise. Atomic Energy of Canada Limited, Technical Record TR-404.*

- Everitt, R.A., and Brown, A. 1986. Subsurface geology of the Underground Research Laboratory: An overview of recent developments. *In* Proceedings of the 20th Information Meeting of the Canadian Nuclear Fuel Waste Management Program. Winnipeg, Manitoba, 1985. Atomic Energy of Canada Limited Technical Record, TR-375.*
- Everitt, R.A., A. Brown, Davison, C.C., Gascoyne, M., and Martin, C.D. 1990. Regional and local setting of the Underground Research Laboratory. *In* Proceedings of the Symposium on Unique Underground Structures, Denver, Colorado, pp. 64-1 to 64-23.
- Farquharson, R.B. 1975. Revised Rb-Sr age of the Lac du Bonnet quartz monzonite, southeastern Manitoba. *Canadian Journal of Earth Sciences*, **12**: 115-118.
- Frape, S.K., Fritz, P., and McNutt, R.H. 1984. Water-rock interaction and chemistry of groundwaters from the Canadian Shield. *Geochimica et Cosmochimica Acta*, **48**: 1617-1627.
- Gascoyne, M. 1989. High levels of uranium and radium in groundwaters at Canada's Underground Research Laboratory, Lac du Bonnet, Manitoba, Canada. *Applied Geochemistry*, **4**: 577-591.
- Gascoyne, M., and Barber, J.H. 1992. The mobility of U, Ra, and Rn in a granitic batholith on the Canadian Shield. *Radiochimica Acta*, **58/59**: 281-284.
- Gascoyne, M. and Chan, T. 1992. Comparison of numerically modelled groundwater residence time with isotopic age data. Proceedings, OECD Workshop on Paleohydrogeological Methods and Their Applications for Radioactive Waste Disposal, Paris, France, Nov. 9-10, 1992.
- Gascoyne, M., and Cramer, J.J. 1987. History of actinide and minor element mobility in an Archean granitic batholith in Manitoba, Canada. *Applied Geochemistry*, **2**: 37-53.
- Gascoyne, M., Davison, C.C., Ross, J.D., and Pearson, R. 1987. Saline groundwaters and brines in plutons in the Canadian Shield. *In* Saline water and gases in crystalline rocks. *Edited* by P. Fritz and S.K. Frape. Geological Association of Canada Special Paper 33, pp. 53-68.
- Gascoyne, M., Sharma, P., and Kubik, P.W. 1994. Origin of groundwater salinity in the Lac du Bonnet granite, southeastern Manitoba, from ^{36}Cl measurements. *Nuclear Instruments and Methods in Physics Research B* 92, pp. 389-392.

- Goodwin, B.W., McConnell, D.B., Andres, T.H., Hajas, W.C., LeNeveu, D.M., Melnyk, T.W., Sherman, G.R., Stephens, M.E., Szekely, J.G., Bera, P.C., Cosgrove, C.M., Dougan, K.D., Keeling, S.B., Kitson, C.I., Kummen, B.C., Oliver, S.E., Witzke, K., Wojciechowski, L., and Wikjord, A.G. (1994). The disposal of Canada's nuclear fuel waste: Postclosure assessment of a reference system. Atomic Energy of Canada Limited Report AECL-10717, COG-93-7.*
- Haimson, B.C. 1990. Stress measurements in the Sioux Falls Quartzite and the state of stress in the midcontinent. *In* Proceedings of the 31st U.S. Symposium on Rock Mechanics, pp. 397-404.
- IUGS (International Union of Geological Sciences) Subcommittee on the Systematics of Igneous Rocks. 1973. Plutonic rocks, classification, and nomenclature. *Geotimes*, **18**(10): 26-30.
- Kamineneni, D.C., Brown, A., Peterman, Z., and Stone, D. 1990a. Radiometric ages, cooling rates and deformation of two granitic plutons in the Superior Province, Canadian Shield. Geological Society of America, Abstracts with Program **22**(7): A244.
- Kamineneni, D.C., Stone, D., and Peterman, Z.E. 1990b. Early Proterozoic deformation in the western Superior Province, Canadian Shield. Geological Society of America Bulletin, **102**: 1623-1634.
- Krogh, T.E., Davis, G.L., Ermanovics, I., and Harris, N.B.W. 1976. U-Pb isotopic ages of zircons from the Berens block and English River gneiss belt. Proceedings of 1976 Geotraverse Conference, University of Toronto, **12-1**, 46.
- MacLeod, I.N. 1980. A gravity survey of Lac de Bonnet Batholith research area RA-3, Lac du Bonnet, Manitoba. Applied Geoscience Branch, Whiteshell Laboratories, Pinawa, Manitoba, unpublished report.
- Martin, C.D. 1989. Characterizing in situ stress domains at the Underground Research Laboratory. *In* Proceedings of the 42nd Canadian Geotechnical Conference, Winnipeg, MB, 1989, 61-74.
- Martin, C.D. and Simmons, G.R. 1992. The Underground Research Laboratory: An opportunity for basic rock mechanics. *International Society for Rock Mechanics News Journal*, **1**: 4-12.
- McCrank, G.F.D. 1985. A geological survey of the Lac du Bonnet Batholith, Manitoba. Atomic Energy of Canada Limited, Report AECL-7816.*
- McCrank, G.F.D., Misiura, J.D., and Brown, P.A. 1981. Plutonic rocks in Ontario. Geological Survey of Canada, Paper 80-23.

- McRitchie, W.D. 1971. The petrology and environment of the acidic plutonic rocks of the Wanipigow - Winnipeg Rivers region, southeastern Manitoba. *In* Geology and geophysics of the Rice Lake region, southeastern Manitoba (Project Pioneer). *Edited by* W. D. McRitchie and W. Weber. Manitoba Mines Branch, Publication 71-1, pp. 7-61.
- Osmani, I.A. 1991. Proterozoic mafic dike swarms in the Superior Province of Ontario. *In* Geology of Ontario. *Edited by* P.C. Thurston, H.R. Williams, R.H. Sutcliffe, and G.M. Stott. Ontario Geological Survey Special Volume 4, Part 1, pp. 661-682.
- Penner, A.P. and Clark, G.S. 1971. Rb-Sr determinations from the Bird River area, southeastern Manitoba. *In* Geoscience studies in Manitoba. *Edited by* A.C. Turnock. Geological Association of Canada, Special Paper 9, pp. 105-109.
- Read, R.S., and Martin, C.D. 1992. Monitoring the excavation-induced response of granite. *In* Proceedings of the 33rd U.S. Symposium on Rock Mechanics, Santa Fe, NM. *Edited by* J.R. Tillerson and W.R. Wawersik, pp. 201-210.
- Read, R.S., and Martin, C.D. 1996. Technical summary of AECL's Mine-by Experiment, Phase 1: Excavation response. Atomic Energy of Canada Limited Report, AECL-11311*.
- Read, R.S., Martin, C.D., and Dzik, E.J. 1995. Asymmetric borehole breakouts at the URL. *In* Proceedings of the 35th U.S. Symposium on Rock Mechanics, Lake Tahoe, NV. *Edited by* J.J.K. Daemen and R.A. Schultz, pp. 879-884.
- Simmons, G.R., Bilinsky, D.M., Davison, C.C., Gray, M.N., Kjartanson, B.H., Martin, C.D., Peters, D.A., Keil, L.D., and Lang, P.A. 1992. Program of experiments for the operating phase of the Underground Research Laboratory. Atomic Energy of Canada Limited, Report AECL-10554.*
- Stone, D., Kamineni, D.C., and Brown, A. 1984. Geology and fracture characteristics of the Underground Research Laboratory lease near Lac du Bonnet, Manitoba. Atomic Energy of Canada Limited, Technical Record TR-243.*
- Stone, D., Kamineni, D.C., Brown, A., and Everitt, R. 1989. A comparison of fracture styles in two granite bodies of the Superior Province. *Canadian Journal of Earth Sciences*, 26: 387-403.
- Thurston, P.C. 1991. Geology of Ontario: Introduction. *In* Geology of Ontario. *Edited by* P.C. Thurston, H.R. Williams, R.H. Sutcliffe, and G.M. Stott. Ontario Geological Survey Special Volume 4, Part 1, pp. 3-26.

Tomsons, D.K., Lodha, G.S., Street, P.J., and Auger, S.L.F. 1995. A Bouguer gravity anomaly map and integrated interpretation of the Whiteshell Research Area, south eastern Manitoba. Atomic Energy of Canada Limited, Technical Record TR-633.*

Trueman, D.L. 1980. Stratigraphic, structural and metamorphic petrology of the Archean greenstone belt at Bird River, Manitoba. Unpublished Ph.D. thesis, University of Manitoba, Winnipeg, Canada.

Whitaker, S.H. 1987. Geoscience research for the Canadian Nuclear Fuel Waste Management Program. Radioactive Waste Management and the Nuclear Fuel Cycle, 8: 145-196.

* Copies are available from the Scientific Document Distribution Office, Atomic Energy of Canada Limited, Chalk River, Ontario K0J 1J0 Canada.

WINNIPEG'96 GUIDEBOOK ORDER FORM

- A1. Evolution of the Thompson Nickel Belt, Manitoba: Setting of Ni-Cu Deposits in the Western Part of the Circum Superior Boundary Zone**
W. Bleeker and J. Macek.....\$12.00 x no. of copies: _____
- A2. Late Holocene Environmental Changes in Southern Manitoba**
E. Nielsen, K. D. McLeod, E. Pip and J.C. Doering..... \$8.00 x no. of copies: _____
- A3. Petrology and Mineralization of the Tanco Rare-Element Pegmatite, Southeastern Manitoba.**
P. Cerny, S. Ercit and P. Vanstone.....\$12.00 x no. of copies: _____
- A4. Lithostratigraphic Assembly of the Eastern Rice Lake Greenstone Belt and Structural Setting of Gold Mineralization at Bissett, Manitoba.**
K.H. Poulson, W. Weber, R. Brommecker and D.Seneshen.....\$13.00 x no. of copies: _____
- A5/B6. Western Superior Transects: Wabigoon-Quetico-Shebandowen and English River-Winnipeg River-Wabigoon**
G. Beakhouse, G. Stott, C. Blackburn, F.W. Breaks, J. Ayer, D. Stone, C. Farrow and F. Corfu.....\$13.00 x no. of copies: _____
- B1. Tectonic Assembly of the Paleoproterozoic Flin Flon Belt and Setting of VMS Deposits**
E. Syme, A. Bailes and S.Lucas.....\$15.00 x no. of copies: _____
- B2. Geomorphic and Sedimentological History of the Central Lake Agassiz Basin.**
J. Teller, H. Thorleifson and G. Matile.....\$14.00 x no. of copies: _____
- B3. Physical Volcanology, Hydrothermal Alteration and Massive Sulphide Deposits of the Sturgeon Lake Caldera**
R. Morton, G. Hudak and E. Koopman.....\$10.00 x no. of copies: _____
- B4. Lower to Middle Paleozoic Stratigraphy of Southwestern Manitoba**
R. Bezys and H. R. McCabe.....\$12.00 x no. of copies: _____
- B5. Geology of the Lac du Bonnet Batholith, Inside and Out: AECL's Underground Research Laboratory, S. E. Manitoba**
R. Everitt, J. McMurry, C. Davison and A. Brown..... \$10.00 x no. of copies: _____
- B7. Industrial Minerals of S.E.Manitoba**
B. Schmidtke and J. Bamburak.....\$3.00 x no. of copies: _____

The entire set may be purchased for \$95.00

	Subtotal:	
	+GST (7%)	
	+Postage and Handling	
	TOTAL	

Orders should be sent to:

Geological Association of Canada, Winnipeg Section
 c/o Geological Services Branch, Manitoba Energy and Mines
 1395 Ellice Ave., Suite 360
 Winnipeg, Manitoba R3G 3P2

Make cheques or money orders payable to "GAC-MAC '96". Add \$2.00 per book for postage and handling. For entire set add \$10.00.

